

Vibrational nonequilibrium in a supersonic expansion with reaction: Application to O₂-O

Bernie D. Shizgal and François Lordet

Department of Chemistry, University of British Columbia, Vancouver, British Columbia V6T 1Z1, Canada

(Received 18 September 1995; accepted 14 November 1995)

The hypersonic expansion of O₂ through a nozzle is considered. The steady nonequilibrium vibrational distribution function of O₂, and the nonequilibrium forward reaction rate coefficient for the dissociation of O₂ are calculated theoretically. In the first instance, the vibrational relaxation of O₂ in the absence of reaction is examined in the temperature range 500–2500 K. The master equation for the vibrational populations, coupled to the steady one-dimensional conservation equations is solved numerically. The vibrational population obtained in this way, is compared to the distribution calculated using either a Treanor model or a Boltzmann distribution characterized by a vibrational temperature. The transition probabilities between O₂ vibrational levels employed take into account the vibrational anharmonicity, and the anisotropic intermolecular potential. For the temperature range 2500–5000 K, the vibrational relaxation including dissociation and recombination is studied. The reactive probabilities that are required for this calculation were obtained from the model of Kiefer and Hajduk [Chem. Phys. **38**, 329 (1979)]. © 1996 American Institute of Physics. [S0021-9606(96)00908-3]

I. INTRODUCTION

The study of the relaxation to a steady state of an initially nonequilibrium vibrational distribution of some molecular system, is a fundamental problem in chemical physics with many applications. Over 30 years ago, Shuler and co-workers¹ pioneered a theoretical description of the relaxation of a nonequilibrium vibrational distribution function of diatomics dilutely dispersed in a large excess of an inert gas which acts as a constant temperature heat bath. This work was extended to other systems by subsequent researchers.² The nonequilibrium vibrational distribution function is given by a master equation,³ which could include vibration–vibration (*V*–*V*) and translation–vibration (*T*–*V*) energy transfers, as well as the effects of reactive processes. A theoretical study of the extent of the departure of the vibrational distribution from equilibrium, and the concomitant departure of reactive rate coefficients from their equilibrium values requires accurate microscopic inelastic, and reactive transition probabilities in the master equation. In addition, the master equation could be coupled to the flow field, which can take on different forms depending on the physical situation, such as for shock waves or nozzle expansions. This requires that the master equation is coupled to the equations describing the flow field. The theoretical treatment of such systems has a very long history. There have been numerous approximate theories, either for the collisional dynamics or with regard to the coupling of vibrational disequilibrium and reaction. In addition, the coupling of the nonequilibrium system to a flow field may or may not be included.

A rigorous treatment of such systems involves the calculation of realistic collision cross sections⁴ derived from accurate potential energy surfaces⁵ of the colliding molecules, and/or atoms. If translational and rotational equilibrium are assumed, the vibrational inelastic rate coefficients in the master equation are then the averages of the corresponding

vibrational inelastic cross sections over the equilibrium rotational and translational distributions. The main objective of such studies is to compare measured and calculated vibrational relaxation times, and/or the time evolution of individual vibrational states.⁶ There has also been considerable interest in the coupling of vibrational relaxation and reactive processes.⁷ This is a very broad subject and the references provided are not meant to be exhaustive of the field but just representative. There are several texts and review articles that have summarized advances in this field.⁸

Interest in this subject has continued to the present. Haug and Truhlar⁹ recently considered the nonequilibrium dissociation rate coefficient for the Ar+H₂→Ar+2H reaction. They considered the solution of the master equation for the H₂ vibrational–rotational distribution function. The vibrational nonequilibrium dissociation of Br₂ in collisions with Ar and Br atoms was considered by Itoh *et al.*¹⁰ Gonzales and Varghese¹¹ studied the nonequilibrium effects in shock heated Ar–O₂ and Ar–H₂ systems. In recent years, there is an active interest to study the vibrational relaxation coupled to reactive processes in flowing systems, such that occur in shock tubes and nozzles.¹² This is an important research area with many applications to a wide variety of subjects involving nonequilibrium gas flows, gas dynamic lasers,^{13,14} combustion processes,¹⁵ plasma processing of materials,¹⁶ atmospheric science, reentry of space vehicles into planetary atmospheres¹⁷ and other applications.

The main objective of this paper is to calculate the vibrational distribution function, and the nonequilibrium forward reaction rate coefficients for the dissociation of O₂ expanded through a nozzle. This requires that the master equation be coupled to the equations describing the flow field. In this paper, we do not consider a time dependent problem but are only concerned with the steady state situation. In the present study, the nonequilibrium phenomena are

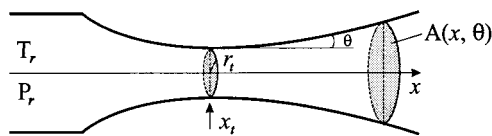


FIG. 1. The one-dimensional nozzle.

generated by a rapid hypersonic expansion. Figure 1 is a depiction of the physical system considered, consisting of a reservoir leading to an axisymmetric hyperbolic nozzle with cross sectional area distribution $A(x, \theta)/A_t = 1 + x^2[\tan(\theta)/r_t]^2$ where r_t is the throat radius, $A_t = \pi r_t^2$ is the throat cross-sectional area, θ is the semi-angle of the asymptotic cone and the subscript t denotes the values at the throat. Typical dimensions of such nozzles are $\theta = 10^\circ$ and $r_t = 3$ mm. The gas is initially in equilibrium at the reservoir temperature and expands in the x direction through the nozzle. All along the nozzle, the flow velocity increases, and the temperature drops rapidly. As a result, vibrational relaxation and recombination occur through atom–molecule and molecule–molecule interactions. Since for O_2 molecules, the dissociation processes are negligible at temperatures lower than 2500 K, we first study vibrational relaxation in the absence of reaction. For temperatures above 2500 K, dissociation and recombination are included. In an earlier paper by one of the present authors,¹⁸ the vibrational nonequilibrium coupled to reaction, and the flow field in a shock tube of uniform cross sectional area was studied. This paper is an extension of this earlier effort, and considers the nonequilibrium vibrational effects including reaction as determined from a solution of the master equation, and coupled to the flow field of an expanding nozzle.

The collisional dynamics of atom–molecule and molecule–molecule collisions are required for the microscopic inelastic rate coefficients in the master equation. This is an important aspect of this subject and has received a lot of attention.^{4,19} The calculation of the collision cross sections for these processes requires the intermolecular potential between the colliding particles, and the solution of the classical or quantum equations of motion. There have been many approximate treatments as well as rigorous close-coupled calculations for simple systems. The classic model is the distorted wave Born quantum calculations of Jackson and Mott²⁰ for the head-on collision of the atom and diatomic. The diatom vibrational states are given by the harmonic oscillator approximation and an exponential interaction potential between the atom and diatomic is assumed. The vibrational transition probabilities are directly proportional to the vibrational quantum number and only single quantum transitions occur. For this collisional model, the distribution function, if initially Boltzmann at the vibrational temperature, relaxes through a series of Boltzmann distributions.²¹ The relaxation of the average vibrational energy takes on a very simple form as derived by Landau and Teller,²² and the vibrational relaxation time was calculated theoretically by Schwartz, Slawsky, and Herzfeld.²³ There have been numerous improvements on this model to include anharmonic ef-

fects, and a three-dimensional model for the atom–diatomic collision.^{19,24} Treanor *et al.*²⁵ considered a master equation with strong ($V-V$) pumping mechanism and derived, with a Chapman–Enskog approach, a quasi-steady distribution which gives an overpopulation relative to a Boltzmann distribution referred to as the Treanor distribution.

In this paper, we employ vibrational inelastic rate coefficients for $O-O_2$ and O_2-O_2 collisions as given by the formalism introduced by Méolans and Chauvin.²⁶ Their model is based on the distorted wave Born approximation and includes the effects of the anharmonicity of molecular vibration, and the anisotropy of the intermolecular potential. They originally applied the theory to N_2-N_2 collisions and it was also previously used by Lordet *et al.*¹⁸ for $O-O_2$ and O_2-O_2 collisions.

At higher temperatures, the gas is partially dissociated, and the vibrational relaxation is coupled to dissociation and recombination. The *ab initio* calculation of the microscopic reactive rate coefficients from specific vibrational–rotational states is a formidable calculation. Alternate semiempirical models for the dependence of microscopic dissociation rate coefficients on the vibrational state have been proposed by numerous researchers^{27–36} that do provide parametrized models for macroscopic rates that can be fitted to experimental data. Another important concern is the way in which the reaction perturbs the Boltzmann distribution, and in turn the effect of this nonequilibrium distribution on the macroscopic rate of reaction. Hammerling *et al.*,²⁷ and later Marrone and Treanor^{28,29} proposed a microscopic reactive rate coefficient that depends exponentially on the vibrational energy. Marrone and Treanor also modified the Landau–Teller model by including the effect of dissociation, and recombination on the time rate of change of the average vibrational energy. Kiefer and Hajduk (KH)³⁰ have proposed a microscopic rate coefficient based on the information theoretic arguments by Kafri and Levine³¹ and by Rebeck and Levine.³² The main concern is the determination of the dependence of the microscopic rate coefficient on the vibrational energy; whether it is constant for all vibrational states or if there is preferential dissociation from higher or lower states. The dependence of these microscopic rate coefficients on the vibrational energy is controlled by an empirical parameter referred to as the “vibrational bias parameter.” This parameter is determined by fitting experimental data to the temperature dependence of macroscopic rate coefficients, obtained by averaging over vibrational states. In this paper, the model established by KH is used, but the vibrational bias parameter is determined in a way different from that proposed by them. It is also shown that this model is similar to the one developed earlier by Marrone and Treanor.²⁹ Park³⁷ proposed a model for the macroscopic rate coefficient that has the usual Arrhenius form but with the temperature replaced with $T_a = T^s T_{\text{vib}}^{1-s}$ where T and T_{vib} are the translational and vibrational temperatures, respectively, and s is chosen between 0.5 and 0.7. This model does not specify the form of the microscopic reactive rate coefficients from specific internal states.

Given the set of microscopic inelastic²⁶ and reactive rate coefficients,³⁰ the vibrational distribution function is deter-

mined from a numerical solution of the master equation, which is coupled to the steady one-dimensional conservation equations for the physical situation shown in Fig. 1. The vibrational distribution function, gas density, temperature, pressure, and reactive rate coefficients are determined numerically as a function of the cross sectional area of the nozzle. In this paper, the vibrational distribution calculated from the master equation is compared to the vibrational distribution of Treanor *et al.*,²⁵ as well as with a Boltzmann distribution function characterized by a vibrational temperature T_{vib} . Previous efforts have either considered vibrational relaxation in a flow field without coupling to reactive processes^{17,38} or the coupled relaxation, and dissociation in the absence of a flow field.⁷ Studies of the coupled vibration and reaction in a flow field were also considered³⁹ but with the model of Marrone and Treanor.^{28,29}

The main objectives of this paper are to study vibrational relaxation without reaction, and then to consider the coupling between vibrational relaxation and reactive processes of O_2 and O expanding through a nozzle. The influence of the (V - V) exchanges and anharmonicity effects on the vibrational distribution are studied. The kinetic and the conservation equations are presented in Sec. II. In Sec. III, we describe the details of the calculation of the inelastic (bound-bound) and reactive (bound-free) transitions for O_2 - O_2 and O_2 - O collisions. The details of the calculation of the population distribution obtained from the master equation is presented in Sec. IV. In Sec. V, we present the calculation of the vibrational distribution function in the absence of reaction obtained from a Treanor *et al.*²⁵ and a Landau-Teller model.²² The results and their discussion are presented in Sec. VI.

II. KINETIC AND CONSERVATION EQUATIONS

The relaxation of diatomic molecules is characterized by different time scales, $\tau_{\text{trans}}, \tau_{\text{rot}}, \tau_{\text{vib}}$, for the translational, rotational, and vibrational degrees of freedom, respectively. Stupochenko *et al.*¹³ have shown that if in addition dissociation occurs, with a characteristic time τ_{diss} , then one generally finds that $\tau_{\text{trans}} < \tau_{\text{rot}} \ll \tau_{\text{vib}} < \tau_{\text{diss}}$. In this paper, we assume that an equilibrium translational-rotational distribution exists during vibrational relaxation and dissociation. We are primarily interested in the nonequilibrium vibrational distribution and the coupling to reaction. The physical situation of interest is shown in Fig. 1. The gaseous O_2 and O mixture is at equilibrium in the reservoir on the left-hand side and allowed to expand in the positive x direction through a nozzle with a cross sectional area specified by $A(x)$. The main purpose of this paper is to study the nonequilibrium behavior for this system expanding through such a nozzle. The gas flow satisfies the set of fluid dynamic equations expressing conservation of mass, momentum, and energy. It is assumed that the lateral variations normal to the x direction are negligible and the steady flow variables depend only on x .

For steady flow, the quasi-one-dimensional conservation equations are of the form,¹³

$$\frac{\partial \rho A u}{\partial x} = 0, \quad (1)$$

$$\frac{\partial P}{\partial x} = -\rho u \frac{\partial u}{\partial x}, \quad (2)$$

$$h + u^2/2 = h_r, \quad (3)$$

where $\rho(x) = \rho_{\text{O}_2}(x) + \rho_{\text{O}}(x) = n(x)M_{\text{O}_2} + n_{\text{O}}(x)M_{\text{O}}$ is the mass density, ρ_{O_2} and ρ_{O} are the mass density, M_{O_2} and M_{O} are the molecular masses and n and n_{O} are the number densities of O_2 and O , respectively. The flow velocity is $u(x)$, $P(x)$ is the pressure, $h(x)$ is the enthalpy of the gas mixture per unit mass, and h_r is the reservoir enthalpy. These macroscopic equations are coupled to the vibrational distribution through the enthalpy. If the vibrational distribution function $n_v(x)$ is normalized to the number density $n(x)$, that is,

$$\sum_v n_v(x) = n(x), \quad (4)$$

then we have

$$h(x) = Y_{\text{O}_2}[C_{\text{O}_2}T + \bar{E}_{\text{vib}}] + Y_{\text{O}}[C_{\text{O}}T + h^0], \quad (5)$$

where $Y_{\text{O}_2} = \rho_{\text{O}_2}/\rho$ and $Y_{\text{O}} = \rho_{\text{O}}/\rho$ are the O_2 and O mass fractions, respectively. The O_2 translation-rotation specific heat at constant pressure per unit mass is $C_{\text{O}_2} = 7\hat{R}/(2\hat{M}_{\text{O}_2})$ and $C_{\text{O}} = 5\hat{R}/(2\hat{M}_{\text{O}})$ is the O translational specific heat at constant pressure per unit mass. $\hat{M}_{\text{O}_2} = N_A M_{\text{O}_2}$ and $\hat{M}_{\text{O}} = N_A M_{\text{O}}$ are the molar masses of O_2 and of O , respectively. $\hat{R} = kN_A = 8.3143 \text{ J K}^{-1} \text{ mol}^{-1}$ is the universal gas constant, k is the Boltzmann constant and N_A is the Avogadro number. \bar{E}_{vib} is the vibrational energy per unit mass that is, $\bar{E}_{\text{vib}} = E_{\text{vib}}/M_{\text{O}_2}$, where

$$E_{\text{vib}} = \frac{1}{n} \sum_v n_v \epsilon_v \quad (6)$$

is the average vibrational energy and h^0 is the standard enthalpy of formation of O .

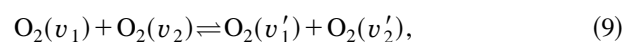
With the definition $R = \hat{R}/\hat{M}_{\text{O}_2}$ and the relations $Y_{\text{O}_2} + Y_{\text{O}} = 1$ and $\hat{M}_{\text{O}_2} = 2\hat{M}_{\text{O}}$, the enthalpy given by Eq. (5) can be expressed as

$$h(x) = \left(\frac{7}{2} + \frac{3}{2}Y_{\text{O}}\right)RT + (1 - Y_{\text{O}})\bar{E}_{\text{vib}} + Y_{\text{O}}h^0. \quad (7)$$

In this way, the macroscopic fluid equations are coupled to the microscopic vibrational distribution function through \bar{E}_{vib} . Similarly, the ideal gas equation of state $P = (n_{\text{O}} + n)kT$, used to close the system of conservation equations, can be written as

$$P = \rho RT(1 + Y_{\text{O}}). \quad (8)$$

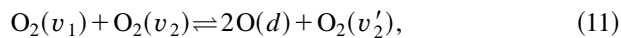
In this study, the vibrational relaxation and dissociation of molecular oxygen is considered. We include molecule-molecule collisions



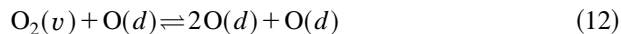
where v_1 is a vibrational quantum number, involving $T-V$ and $V-V$ energy exchanges characterized by a cross section, $\overline{\sigma_{v_1 \rightarrow v'_1}^{v_2 \rightarrow v'_2}}$, for the forward collision process. Atom-molecule collisions



involving $T-V$ energy exchanges, characterized by cross sections $\sigma_{v \rightarrow v'}$, are also included. The cross sections for the reverse processes are given by microscopic reversibility.⁴⁰ We also include molecule-molecule collisions



involving reactive transitions producing two oxygen atoms characterized by the cross section $\overline{\sigma_{v_1 \rightarrow d}^{v_2 \rightarrow v'_2}}$, for the forward collision process, where d denotes the electronic ground state of an O atom. Reactive atom-molecule collisions



are characterized by the cross section $\sigma_{v \rightarrow d}$. The spatial variation of the vibrational population in a hypersonic flow for which collisional processes Eqs. (9)–(12) are assumed, is governed by a master equation for the moving fluid of the form

$$\begin{aligned} \frac{\partial n_{v_1} u A}{\partial x} = & \frac{AZ_{11}}{n} \left[\sum_{v_2, v'_1, v'_2} (-n_{v_1} n_{v_2} P_{v_1 \rightarrow v'_1}^{v_2 \rightarrow v'_2} + n_{v_1} n_{v'_2} P_{v'_1 \rightarrow v_1}^{v_2 \rightarrow v_2}) \right. \\ & \left. + \sum_{v_2, v'_2} (-n_{v_1} n_{v_2} P_{v_1 \rightarrow d}^{v_2 \rightarrow v'_2} + n_{\text{O}}^2 n_{v'_2} P_{d \rightarrow v_1}^{v_2 \rightarrow v_2}) \right] \\ & + AZ_{12} \left[\sum_{v'_1} (-n_{v_1} P_{v_1 \rightarrow v'_1} + n_{v'_1} P_{v'_1 \rightarrow v_1}) \right. \\ & \left. + (-n_{v_1} P_{v_1 \rightarrow d} + n_{\text{O}}^2 P_{d \rightarrow v_1}) \right], \quad (13) \end{aligned}$$

where Z_{11} and Z_{12} are the $\text{O}_2\text{-O}_2$ and O-O_2 collision frequencies, respectively, given by

$$\begin{aligned} Z_{11} = & n \left(\frac{8kT}{\pi\mu_{11}} \right)^{1/2} \left(\sum_{v_1, v'_1, v_2, v'_2} \overline{\sigma_{v_1 \rightarrow v'_1}^{v_2 \rightarrow v'_2}} + \sum_{v_1, v_2, v'_2} \overline{\sigma_{v_1 \rightarrow d}^{v_2 \rightarrow v'_2}} \right. \\ & \left. + \overline{\sigma_{e,11}} \right), \quad (14) \end{aligned}$$

$$Z_{12} = n_{\text{O}} \left(\frac{8kT}{\pi\mu_{12}} \right)^{1/2} \left(\sum_{v_1, v'_1} \overline{\sigma_{v_1 \rightarrow v'_1}} + \sum_{v_1} \overline{\sigma_{v_1 \rightarrow d}} + \overline{\sigma_{e,12}} \right). \quad (15)$$

In Eqs. (14) and (15), μ_{11} and μ_{12} are the reduced masses of the pair $\text{O}_2\text{-O}_2$ and O-O_2 , respectively, $\overline{\sigma_{e,11}}$ and $\overline{\sigma_{e,12}}$ are the elastic hard sphere cross sections. The overbars on the cross sections signify the average over an equilibrium translational-rotational distribution function at the temperature T . In Eq. (13), the first summation represents $T-V$ and

$V-V$ energy exchanges involving collisions given by Eq. (9). The second summation represents reactive transitions involving collisions given by Eq. (11), the third summation $T-V$ energy exchanges given by Eq. (10), and the fourth summation reactive transitions given by Eq. (12). The probability for forward transitions, $P_{v_1 \rightarrow v'_1}^{v_2 \rightarrow v'_2}$ and $P_{v_1 \rightarrow v'_1}$ that occur in the master equation, Eqs. (13) are given by

$$\begin{aligned} P_{v_1 \rightarrow v'_1}^{v_2 \rightarrow v'_2} = & \overline{\sigma_{v_1 \rightarrow v'_1}^{v_2 \rightarrow v'_2}} \left/ \left(\sum_{v_1, v'_1, v_2, v'_2} \overline{\sigma_{v_1 \rightarrow v'_1}^{v_2 \rightarrow v'_2}} \right. \right. \\ & \left. \left. + \sum_{v_1, v_2, v'_2} \overline{\sigma_{v_1 \rightarrow d}^{v_2 \rightarrow v'_2}} + \overline{\sigma_{e,11}} \right), \quad (16) \end{aligned}$$

$$P_{v_1 \rightarrow v'_1} = \overline{\sigma_{v_1 \rightarrow v'_1}} \left/ \left(\sum_{v_1, v'_1} \overline{\sigma_{v_1 \rightarrow v'_1}} + \sum_{v_1} \overline{\sigma_{v_1 \rightarrow d}} + \overline{\sigma_{e,12}} \right). \quad (17)$$

The probabilities $P_{v_1 \rightarrow v'_1}^{v_2 \rightarrow v'_2}$ and $P_{v_1 \rightarrow v'_1}$ were employed in the previous paper¹⁸ and discussed in Sec. III A. The probabilities for the forward dissociation transitions, $P_{v_1 \rightarrow d}^{v_2 \rightarrow v'_2}$ and $P_{v_1 \rightarrow d}$, that occur in the master equation, Eqs. (13), are taken from the model of KH³⁰ and are given by

$$\begin{aligned} P_{v_1 \rightarrow d}^{v_2 \rightarrow v'_2} = & \overline{\sigma_{v_1 \rightarrow d}^{v_2 \rightarrow v'_2}} \left/ \left(\sum_{v_1, v'_1, v_2, v'_2} \overline{\sigma_{v_1 \rightarrow v'_1}^{v_2 \rightarrow v'_2}} \right. \right. \\ & \left. \left. + \sum_{v_1, v_2, v'_2} \overline{\sigma_{v_1 \rightarrow d}^{v_2 \rightarrow v'_2}} + \overline{\sigma_{e,11}} \right), \quad (18) \end{aligned}$$

$$P_{v_1 \rightarrow d} = \overline{\sigma_{v_1 \rightarrow d}} \left/ \left(\sum_{v_1, v'_1} \overline{\sigma_{v_1 \rightarrow v'_1}} + \sum_{v_1} \overline{\sigma_{v_1 \rightarrow d}} + \overline{\sigma_{e,12}} \right). \quad (19)$$

The macroscopic rate of reaction is obtained by summing Eq. (13) over all states v_1 . The terms involving vibrational energy exchanges vanish owing to mass conservation for these collision processes. The result is the following macroscopic rate equation:

$$\begin{aligned} \frac{\partial nuA}{\partial x} = & \frac{AZ_{11}}{n} \sum_{v_1, v_2, v'_2} (-n_{v_1} n_{v_2} P_{v_1 \rightarrow d}^{v_2 \rightarrow v'_2} + n_{\text{O}}^2 v_{v'_2} P_{d \rightarrow v_1}^{v_2 \rightarrow v_2}) \\ & + AZ_{12} \sum_{v_1} (-n_{v_1} P_{v_1 \rightarrow d} + n_{\text{O}}^2 P_{d \rightarrow v_1}), \quad (20) \end{aligned}$$

where $[\partial(n_{\text{O}}uA)/\partial x] = -2[\partial(nuA)/\partial x]$ arises from the stoichiometry of Eqs. (11) and (12). Equation (20) can be rewritten in terms of the macroscopic rate equation

$$\frac{\partial nuA}{\partial x} = A[-k_{f,11}n^2 + k_{b,11}nn_{\text{O}}^2 - k_{f,12}nn_{\text{O}} + k_{b,12}n_{\text{O}}^3], \quad (21)$$

where $k_{f,11}$ and $k_{f,12}$ are the macroscopic forward rate coefficients for $\text{O}_2\text{-O}_2$ and $\text{O}_2\text{-O}$ collisions, respectively, and

$k_{b,11}$ and $k_{b,12}$ are the corresponding macroscopic reverse rate coefficients. With Eqs. (20) and (21), one obtains

$$k_{f,11} = \frac{Z_{11}}{n} \sum_{v_1, v_2, v_2'} \frac{n_{v_1} n_{v_2}}{n^2} P_{v_1 \rightarrow d}^{v_2 \rightarrow v_2'}, \quad (22)$$

$$k_{f,12} = \frac{Z_{12}}{n_O} \sum_{v_1} \frac{n_{v_1}}{n} P_{v_1 \rightarrow d}, \quad (23)$$

$$k_{b,11} = \frac{Z_{11}}{n} \sum_{v_1, v_2, v_2'} \frac{n_{v_2'}}{n} P_{d \rightarrow v_1}^{v_2' \rightarrow v_2}, \quad (24)$$

$$k_{b,12} = \frac{Z_{12}}{n_O} \sum_{v_1} P_{d \rightarrow v_1}. \quad (25)$$

In the master equation, the probabilities of the vibrational transitions are related by the principle of detailed balance at equilibrium. For the bound-bound transitions, detailed balancing⁴⁰ is expressed by

$$-n_{v_1}^{\text{eq}} n_{v_2}^{\text{eq}} P_{v_1 \rightarrow v_1'}^{v_2 \rightarrow v_2'} + n_{v_1'}^{\text{eq}} n_{v_2'}^{\text{eq}} P_{v_1' \rightarrow v_1}^{v_2' \rightarrow v_2} = 0. \quad (26)$$

The equilibrium distribution function, n_v^{eq} is given by

$$n_v^{\text{eq}} = \frac{n^{\text{eq}} \exp(-\epsilon_v/kT)}{\sum_v \exp(-\epsilon_v/kT)}, \quad (27)$$

where ϵ_v is the vibrational energy of O_2 in the vibrational level v . The equality of forward and reverse rates for inelastic collisions at equilibrium, Eq. (26), gives the reverse transition probability as a function of the forward transition probability, that is,

$$P_{v_1' \rightarrow v_1}^{v_2' \rightarrow v_2} = \exp[(-\epsilon_{v_1} - \epsilon_{v_2} + \epsilon_{v_1'} + \epsilon_{v_2'})/kT] P_{v_1 \rightarrow v_1'}^{v_2 \rightarrow v_2'}. \quad (28)$$

Similarly, for the bound-free transitions, we have

$$-n_{v_1}^{\text{eq}} n_{v_2}^{\text{eq}} P_{v_1 \rightarrow d}^{v_2 \rightarrow v_2'} + (n_O^{\text{eq}})^2 n_{v_2}^{\text{eq}} P_{d \rightarrow v_1}^{v_2' \rightarrow v_2} = 0. \quad (29)$$

Equation (29) may be rewritten as

$$P_{d \rightarrow v_1}^{v_2' \rightarrow v_2} = \left(\frac{n_{v_1}^{\text{eq}} n_{v_2}^{\text{eq}}}{(n_O^{\text{eq}})^2 n_{v_2'}^{\text{eq}}} \right) P_{v_1 \rightarrow d}^{v_2 \rightarrow v_2'}. \quad (30)$$

We replace the ratio $(n_O^{\text{eq}})^2/n^{\text{eq}}$ in term of the equilibrium rate constant, that is,

$$K^{\text{eq}} = (n_O^{\text{eq}})^2/n^{\text{eq}}. \quad (31)$$

Thus, with Eqs. (27) and (31), Eq. (30) is rewritten as

$$P_{d \rightarrow v_1}^{v_2' \rightarrow v_2} = \left(\frac{\exp[(-\epsilon_{v_1} - \epsilon_{v_2} + \epsilon_{v_2'})/kT]}{K^{\text{eq}}} \right) P_{v_1 \rightarrow d}^{v_2 \rightarrow v_2'}. \quad (32)$$

The transition probabilities in the master equation have thus been defined and a numerical solution of the master equation can be considered. Equations (22)–(25) show that the macroscopic forward and backward reaction rates correspond to an average over the vibrational states of the individual rate coefficients. The calculation of the macroscopic

rates of reaction requires the microscopic forward probabilities of transition, and the nonequilibrium vibrational distribution function. If the processes of vibrational relaxation, dissociation, and recombination did not perturb the vibrational distribution, then n_v/n would be the equilibrium Boltzmann distribution Eq. (27). For the case of a Boltzmann distribution function, Eq. (21) is written as

$$\frac{\partial n u A}{\partial x} = A(-k_{f,11}^{\text{eq}} n^2 + k_{b,11}^{\text{eq}} n n_O^2 - k_{f,12}^{\text{eq}} n n_O + k_{b,12}^{\text{eq}} n_O^3). \quad (33)$$

In Eq. (33), the equilibrium rate constants $k_{f,11}^{\text{eq}}, k_{b,11}^{\text{eq}}, k_{f,12}^{\text{eq}}, k_{b,12}^{\text{eq}}$ have the form given by Eqs. (22)–(25) with the equilibrium distribution given by Eq. (27), and depend only on the temperature. When the gas is in motion, the vibrational distribution function is not in equilibrium. The vibrational relaxation and the reactive processes perturb the vibrational distribution function, and the equilibrium reaction rates do not correspond to the equilibrium value. The ratios

$$F_1 = \frac{k_{f,11}}{k_{f,11}^{\text{eq}}} \quad (34)$$

and

$$F_2 = \frac{k_{f,12}}{k_{f,12}^{\text{eq}}} \quad (35)$$

are the quantities calculated and provide a measure of the departure from equilibrium.

III. RATES FOR THE BOUND-BOUND AND BOUND-FREE TRANSITIONS

The methodology for the study of nonequilibrium effects discussed in Sec. II requires as input the thermally averaged microscopic vibrationally inelastic, and reactive rate coefficients in the master equation given by Eq. (13). In this section, we provide the details of the vibrationally inelastic cross sections for $\text{O}_2\text{-O}_2$ and $\text{O}_2\text{-O}$ collisions that are used. A similar discussion is presented in Sec. III B for the reactive rate coefficients. We assume that the molecules are represented by a Morse oscillator model and the vibrational energy of O_2 in the vibrational level v is given by $\epsilon_v = \omega_e[(v+1/2) - x_e(v+1/2)^2]$ with $\omega_e = 1580 \text{ cm}^{-1}$ and $x_e = 7.64 \times 10^{-3}$.⁴¹

A. Vibrationally inelastic transition probabilities

Theoretical calculations of the $T\text{-}V$ and $V\text{-}V$ energy exchanges in molecule-molecule and atom-molecule collisions have a very long history. The rigorous solution of this problem requires an accurate potential energy surface between the colliding species, and the calculation of the quantum mechanical collision cross sections. For the systems of interest in this study, this is not presently amenable to an exact treatment and approximation is necessary. A good review of the subject up to about 1976 has been presented by Clarke and McChesney.⁸ We do not repeat here a detailed historical account of the developments in this field.

The model adopted in this work is the one used in the recent paper by Lordet *et al.*¹⁸ This model represents an improvement in the Jackson and Mott approach²⁰ in that the anharmonicity and the anisotropic effects are taken into account. In this paper, the calculation of the quantum mechanical cross sections for inelastic O₂-O₂ and O₂-O collisions are based on (i) a distorted wave Born approximation, (ii) a Morse potential for the diatomic molecules, and (iii) an exponential intermolecular interaction between the colliding pair, that is,

$$V(r) = V_0 \exp(-r/l). \quad (36)$$

In Eq. (36), r is the intermolecular separation, l and V_0 measure the range and strength of the interaction, respectively. In this work, the value of l is determined by fitting the vibrational relaxation time to published experimental values. The thermally averaged inelastic cross sections that appear in Eqs. (16) and (17) are calculated with Eqs. (19)–(34) of Ref. 18. The inelastic collision cross sections depend sensitively on the range parameter, l , in the interaction potential Eq. (36) (Ref. 8), but are independent of V_0 .

For O-O₂, we determine the value of l by fitting the calculated value of $\sigma_{1 \rightarrow 0}$ with experimental measurements of the vibrational relaxation time. With the assumption that the Landau-Teller theory²² is applicable, the vibrational relaxation time τ_{12} , is given by,

$$\tau_{12}^{-1} = n_O (8kT/\pi\mu_{12})^{1/2} \overline{\sigma_{1 \rightarrow 0}} [1 - \exp(-\hbar\omega/kT)], \quad (37)$$

where ω is the vibrational frequency and \hbar is Planck's constant. With the ideal gas equation of state, we have that,

$$\overline{\sigma_{1 \rightarrow 0}} = \frac{kT}{\tau_{12}P[1 - \exp(-\hbar\omega/kT)]} (\pi\mu_{12}/8kT)^{1/2}. \quad (38)$$

We use the vibrational relaxation time determined by Park⁴² and expressed in terms of the fitted expression,

$$\tau_{12}P = \exp[47.7(T^{-1/3} - 0.059) - 18.42] \text{ atm s}, \quad (39)$$

where T is in degrees Kelvin. In Fig. 2, we compare the calculated and experimental thermally averaged cross sections normalized to the hard sphere elastic cross section $\sigma_{12,e} = \pi(d_O + d_{O_2})^2/4$, for several different values of l [curves (a)–(c)], where $d_O = 3 \text{ \AA}$ and $d_{O_2} = 3.5 \text{ \AA}$ are the collision diameters of O and O₂,⁴³ respectively. We show the cross sections for $l = 0.155 \text{ \AA}$ [curve (a)]. The least-squares fit to the expression of Park, Eq. (38), gives the value of $l = 0.16 \text{ \AA}$ [curve (b)] over the temperature range 1000 K–5000 K. The results obtained by Park predict high efficiencies for O₂ relaxation by atomic oxygen. The efficiency for vibrational relaxation increases with increasing T , and for O₂-O relaxation, $\overline{\sigma_{1 \rightarrow 0}}/\sigma_{12,e} = 0.3$ at $T \approx 5000 \text{ K}$. We also show the cross sections for $l = 0.2336 \text{ \AA}$ [curve (c)] reported by Radzig and Smirnov⁴⁴ determined from scattering experiments and $l = 0.2487 \text{ \AA}$ [curve (d)] given by Cubbley and Mason⁴⁵ obtained by studies of viscosity coefficients. For O₂-O collisions, these are the same order of magnitude but are not in agreement with those obtained from relaxation experiments.

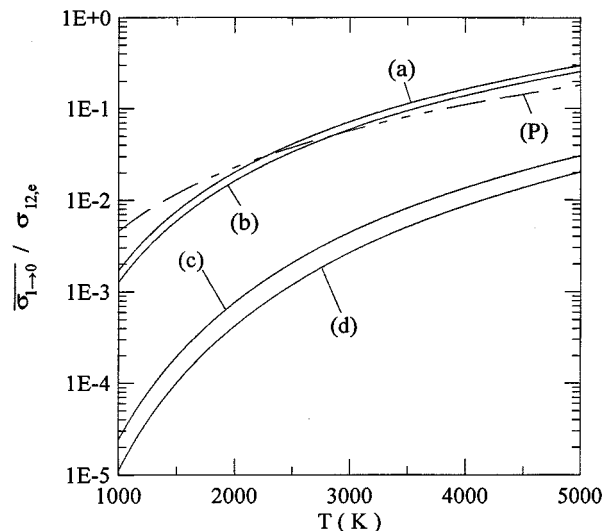


FIG. 2. Cross section $\overline{\sigma_{1 \rightarrow 0}}$ for O₂-O collisions normalized to $\sigma_{12,e}$ for different values of l . (a) $l = 0.155 \text{ \AA}$, (b) $l = 0.16 \text{ \AA}$, (c) $l = 0.2336 \text{ \AA}$. (d) $l = 0.2487 \text{ \AA}$. (P) result from Park⁴² obtained from Eqs. (37) and (38).

There is a wealth of experimental data available for the vibrational relaxation time of pure molecular oxygen. We use the experimental vibrational relaxation time given by Camac⁴⁶ in the form

$$(\tau_{11}P)^{-1} = \{kT^{7/6} 6 \times 10^{-7} [1 - \exp(2228T)] \times \exp[(-10.4 \times 10^6/T)^{1/3}]\} \text{ atm}^{-1} \text{ s}^{-1}, \quad (40)$$

with T in degrees Kelvin, and the results provided by Millikan and White (MW),⁴⁷

$$\tau_{11}P = \exp[1.16 \times 10^{-3} \mu_{11}^{1/2} (\hbar\omega/k)^{4/3} (T^{-1/3} - 0.015 \mu_{11}^{1/4}) - 18.42] \text{ atm s}, \quad (41)$$

where μ_{11} is in kg. We follow a similar procedure for O₂-O₂ collisions and employ the calculated cross sections for single-quantum changes in one of the $\overline{\sigma_{1 \rightarrow 0}} = \overline{\sigma_{1 \rightarrow 0}^{2 \rightarrow 2}}$ as $\overline{\sigma_{1 \rightarrow 0}}$ in Eqs. (37) and (38) with the corresponding reduced mass, μ_{11} and the number density n . In Fig. 3, the inelastic cross sections normalized to a hard sphere elastic cross section $\sigma_{11,e} = \pi d_{O_2}^2$ is plotted against the temperature for different values of l . Fig. 3 shows that the cross section derived from the relaxation times given by MW and Camac (C) (dashed lines) are in very good agreement for low temperatures. However, the discrepancy increases with the temperature and at 5000 K, $\sigma_{1 \rightarrow 0}(C)/\sigma_{1 \rightarrow 0}(MW) \approx 7$. In Fig. 3, we also show the calculated cross sections for several values of l [curve (a)–(e)]. We have included $\overline{\sigma_{1 \rightarrow 0}}$ calculated with $l = 0.3144 \text{ \AA}$ [curve (d)] given by Cubbley and Mason and with $l = 0.3508 \text{ \AA}$ [curve (e)] given by Radzig and Smirnov. An optimum value of $l = 0.256 \text{ \AA}$ [curve (c)] was found to give the best least-squares fit to the expression of Camac, Eq. (40). Moreover, this value of l gives vibrational cross sections for high vibrational states which are in good agreement with those determined by Kunc.⁴⁸ There is a lack of data

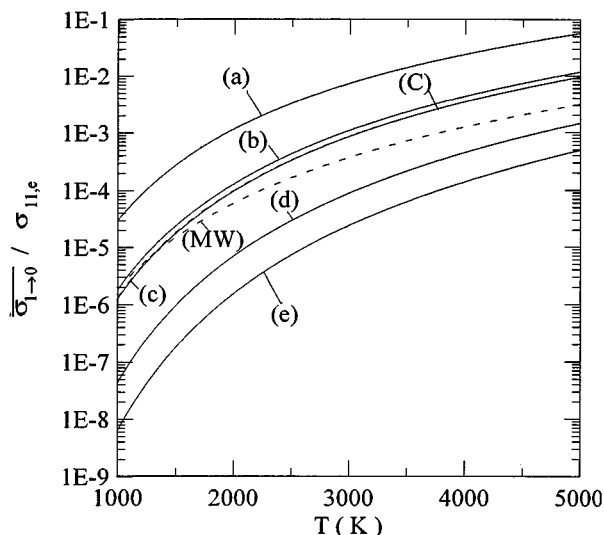


FIG. 3. Cross section $\sigma_{l=0}$ for $\text{O}_2\text{-O}_2$ interactions normalized to $\sigma_{11,e}$ for different l . (a) $l=0.205$ Å, (b) $l=0.25$ Å, (c) $l=0.256$ Å, (d) $l=0.3144$ Å, (e) $l=0.3508$ Å. Millikan and White (MW) (Ref. 45), Camac (C) (Ref. 28).

concerning the $V\text{-}V$ energy exchanges for $\text{O}_2\text{-O}_2$ collisions and our results obtained with the different values of l cannot be compared with other results.

B. Microscopic reactive rate coefficients

The numerical study of hypersonic flow coupled to reaction studied in this paper requires simple analytical expressions for the dependence of the microscopic reaction rate coefficients on the vibrational state of the diatomic and the temperature. A complete treatment of these bound-free transitions requires a three body potential energy surface and intensive numerical calculations of the state-dependent reactive cross sections. Instead, we choose to model the dissociation with simple analytical expressions that have been used by other workers^{33,34} to account for nonequilibrium dissociation coupled with vibrational relaxation. In this paper, for both O-O_2 and $\text{O}_2\text{-O}_2$ collisions, the models suggested by Kiefer and co-workers^{33,30} of the form

$$k_{f,11}(v \rightarrow d, T) = C(T) \exp(\lambda_{11} \epsilon_v / D) \times \exp[-(D - \epsilon_v) / kT], \quad (42)$$

and that of Ramakrishna and Babu (RB),³⁵

$$k_{f,11}(v \rightarrow d, T) = E(T) [1 + (D - \epsilon_v) / kT] \times \exp(\lambda_{11} \epsilon_v / D) \exp[-(D - \epsilon_v) / kT], \quad (43)$$

are employed. In Eq. (42) and (43), D is the dissociation energy and the parameter λ_{11} , referred to as the “vibrational bias”,³⁰ controls the preferential dissociation versus vibrational quantum number. Although we employ Eq. (42) as an empirical model, it can be theoretically justified. This can be considered as the product of two factors, an Arrhenius rate constant $C(T) \exp[-(D - \epsilon_v) / kT]$, referred to as the prior rate constant that can be derived from the statistical approach of Rebick and Levine³² based on prior distribution functions.

The second factor, $\exp(\lambda_{11} \epsilon_v / D)$, which is the vibrational bias, is consistent with surprisal analysis of collision induced dissociation as discussed by Kafri and Levine.³¹ For large values of the vibrational bias, the enhancement of the dissociation rate from the higher vibrational levels is significantly greater than that from the lower levels. For $\text{O}_2\text{-O}_2$ collisions, we assume that there is no change in vibrational quantum number for one of the two molecules in a collision so that we set $P_{v \rightarrow d}^{v_2 \rightarrow v_2'} = P_{v \rightarrow d}^{v_2 \rightarrow v_2} = P_{v \rightarrow d}$. The probability for dissociation is defined consistent with the macroscopic reactive rate coefficient so that we write

$$k_{f,11}(v \rightarrow d, T) = \frac{Z_{11}}{n} P_{v \rightarrow d}, \quad (44)$$

and a similar expression for $k_{f,12}(v \rightarrow d, T)$.

The value of $k_{f,11}(v \rightarrow d, T)$ is completely specified once the pre-exponential factors, $C(T)$ or $E(T)$, and the vibrational bias parameter, λ_{11} , are defined. The pre-exponential factors, $C(T)$ and $E(T)$, are determined by setting the value of the dissociation rate from the topmost vibrational level, denoted by “top,” to some known value which is generally the hard sphere collision rate given by $Q_{11} = (8kT / \pi \mu_{11})^{1/2} \sigma_{e,11}$. We employ two different normalizations of $k_{f,11}(v \rightarrow d, T)$ in Eq. (42) referred to as normalizations A and B, and one normalization in Eq. (43) referred to as normalization C.

For case A, we set the rate coefficient for dissociation for a fictitious vibrational energy, $\epsilon_{\text{top}} = D$, equal to Q_{11} , so that

$$C_A(T) = Q_{11} \exp(-\lambda_{11}). \quad (45)$$

This is similar to the normalization chosen by KH.³⁰ A second choice involves setting the dissociation rate from the topmost level equal to the Arrhenius value without vibrational bias, that is,

$$C_B(T) = Q_{11} \exp(-\lambda \epsilon_{\text{top}} / D). \quad (46)$$

The final choice stems from the model used by RB³⁵ which has a different dependence on vibrational energy, and we have

$$E_C(T) = Q_{11} \exp(-\lambda_{11}). \quad (47)$$

It is important to mention that for O_2 , we have that $(D - \epsilon_{\text{top}}) / k = 775$ K or equivalently $D / \epsilon_{\text{top}} = 1.015$ for a Morse oscillator and $(D - \epsilon_{\text{top}}) / k = 1302$ K and $D / \epsilon_{\text{top}} = 1.022$ for an harmonic oscillator. It is the departure of this last ratio from unity that distinguishes the normalizations A and B. The value of the vibrational bias is now determined by fitting the equilibrium macroscopic rate coefficient to the experimental value, that is,

$$k_{f,11}^{\text{eq}} = \sum_v \frac{n_v^{\text{eq}}}{n^{\text{eq}}} k_{f,11}(v \rightarrow d, T) = A T^m \exp(-D / kT), \quad (48)$$

where $A = 3.32 \times 10^{-9} \text{ m}^3 \text{ mol}^{-1} \text{ s}^{-1}$, $m = -1.5$, and $D / k = 59\,500$ K.³⁷ The normalization of $k_{f,12}(v \rightarrow d, T)$ is carried

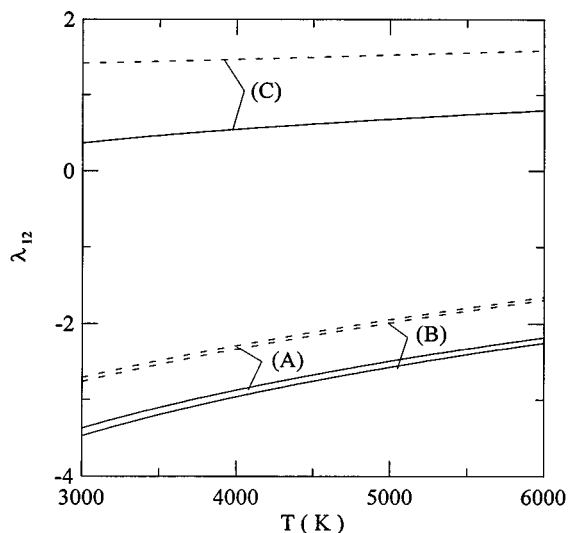


FIG. 4. Vibrational bias parameter λ_{12} for O_2 - O collisions vs temperature. (—) harmonic oscillator model and (---) anharmonic model. Normalization A and model of KH, normalization B and model of KH, normalization C and model of RB.

out in a similar fashion. In this case, λ_{12} characterizes O_2 - O interactions and $A = 1.6604 \times 10^{-8} \text{ m}^3 \text{ mol}^{-1} \text{ s}^{-1}$ and $m = -1.5$.

It is important to recognize that the model of KH in Eq. (42) is the same as that proposed by Marrone and Treanor²⁹ [see Eq. (71) and also Eq. (50) of Ref. 18], where instead of the vibrational bias parameter they introduce a temperature, U_{11} , where $\lambda_{11} = D/kU_{11}$ and $C(T)$ is normalized with Eq. (48).

The temperature dependence of the vibrational bias parameters λ_{12} and λ_{11} for O_2 dissociation by O_2 - O and O_2 - O_2 collisions is shown in Figs. 4 and 5, respectively. The three

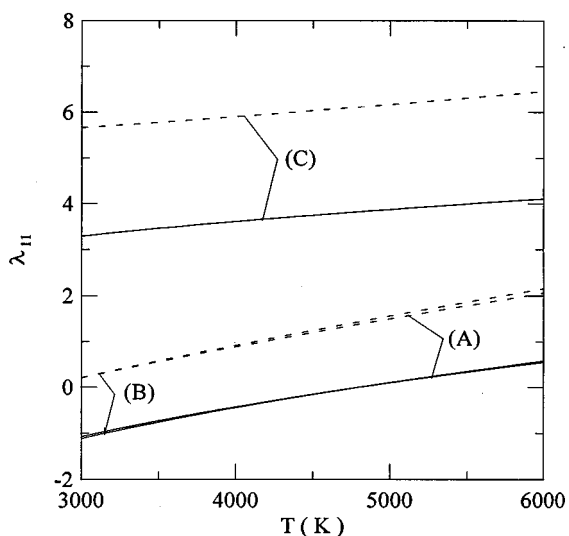


FIG. 5. Vibrational bias parameter λ_{11} for O_2 - O_2 collisions vs temperature. (—) harmonic oscillator model and (---) anharmonic model. Normalization A and model of KH, normalization B and model of KH, normalization C and model of RB.

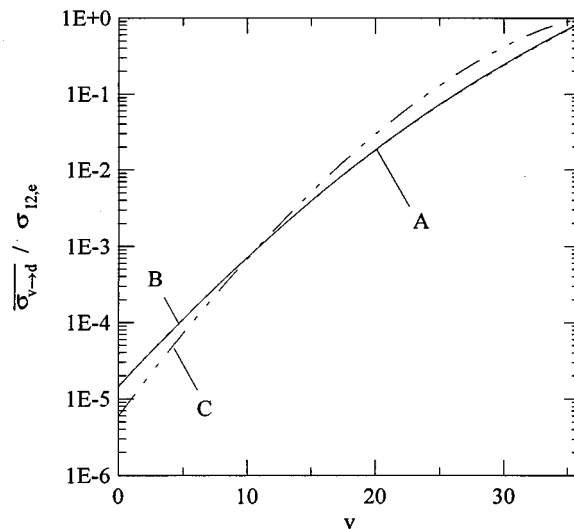


FIG. 6. Microscopic reactive cross section $\overline{\sigma_{v \rightarrow d}}$ for O_2 - O collisions normalized to $\sigma_{12,e}$ vs vibrational level for anharmonic oscillator at $T = 4500 \text{ K}$. Normalization A and model of KH, normalization B and model of KH, normalization C and model of RB.

models predict an increase of the parameters λ_{11} and λ_{12} with increasing temperature. Consequently, for a given vibrational level v , the effect of λ_{11} and λ_{12} is to reduce the reactive cross section with increasing temperature. Nevertheless, λ_{11} and λ_{12} are weak functions of temperature.

In Figs. 4 and 5, the solid curve and the dashed curve are for the harmonic and anharmonic oscillator, respectively. At a given temperature, the vibrational bias parameter calculated with normalizations A [curve (A)], B [curve (B)] and C [curve (C)] is bigger for the anharmonic model than with the harmonic one. Moreover, the vibrational bias parameter calculated with normalization (A) and (B) are very close whatever is the temperature.

In Figs. 6 and 7, the normalized reactive cross sections $\overline{\sigma_{v \rightarrow d}} / \sigma_{12,e}$ and $\overline{\sigma_{v \rightarrow d}} / \sigma_{22,e}$ are plotted at 4500 K for O_2 - O and O_2 - O_2 collisions, respectively. The reactive cross sections obtained with the model of KH and normalizations A [curve (A)] and B [curve (B)] are very close to each other whatever is the vibrational level, whereas the reactive cross sections calculated with the model of RB and normalization C are smaller for $v \leq 10$ compared to those of the model of KH. All the reactive cross sections are of the same order of magnitude among the vibrational levels with $v \approx 10$. Concerning the vibrational states with $v \geq 10$, the model of RB predicts larger reactive cross sections than those calculated with the model of KH. In addition, $C(T)$ and $E(T)$ are calculated in such a way that near the dissociation limit, for $v = 37$, the different reactive cross sections are close to the hard sphere cross sections.

IV. NUMERICAL SOLUTION OF THE COUPLED FLUID AND MASTER EQUATION

A. Without reaction

In the absence of reaction, the master equation given by Eq. (13) may be rewritten as

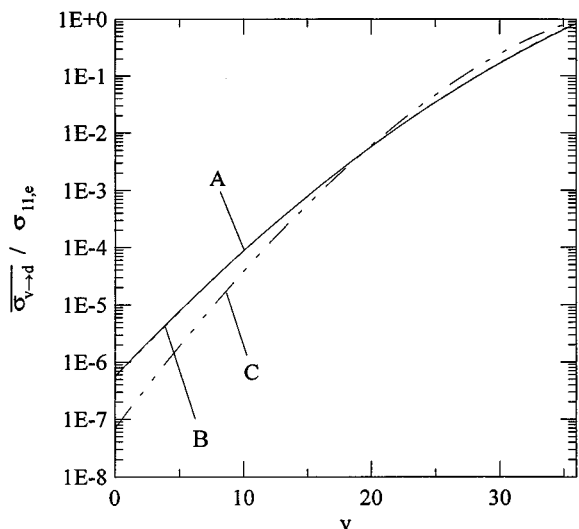


FIG. 7. Microscopic reactive cross section $\overline{\sigma_{v \rightarrow d}}$ for O_2 - O_2 collisions normalized to $\sigma_{11,e}$ vs v at $T=4500$ K. Normalization A and model of KH, normalization B and model of KH, normalization C and model of RB.

$$\frac{1}{nAu} \frac{\partial n_{v_1} uA}{\partial x} = \frac{Z_{11}}{u} \sum_{v_2, v'_1, v'_2} \left(-\frac{n_{v_1} n_{v_2}}{n^2} P_{v_1 \rightarrow v'_1}^{v_2 \rightarrow v'_2} + \frac{n_{v'_1} n_{v'_2}}{n^2} P_{v'_1 \rightarrow v_1}^{v'_2 \rightarrow v_2} \right). \quad (49)$$

The equation of mass conservation, Eq. (1), is obtained by summing Eq. (13) over all states v_1 ,

$$\frac{\partial nuA}{\partial x} = 0. \quad (50)$$

From Eq. (50), since (nAu) is independent of x , the left-hand side of Eq. (49) may be rearranged to give

$$\frac{1}{nAu} \frac{\partial n_{v_1} uA}{\partial x} = \frac{\partial (n_{v_1}/n)}{\partial x}. \quad (51)$$

Thus, the master equation, Eq. (49), may be rewritten in the form

$$\frac{\partial (n_{v_1}/n)}{\partial x} = \frac{Z_{11}}{u} \sum_{v_2, v'_1, v'_2} \left(-\frac{n_{v_1} n_{v_2}}{n^2} P_{v_1 \rightarrow v'_1}^{v_2 \rightarrow v'_2} + \frac{n_{v'_1} n_{v'_2}}{n^2} P_{v'_1 \rightarrow v_1}^{v'_2 \rightarrow v_2} \right). \quad (52)$$

The rate of change of the vibrational energy equation is obtained by multiplying Eq. (52) by ϵ_{v_1} and summing over v_1 .

The variation of the vibrational energy with x is given by

$$\frac{\partial E_{\text{vib}}}{\partial x} = \frac{Z_{11}}{u} \sum_{v_1, v_2, v'_1, v'_2} \left(-\frac{n_{v_1} n_{v_2}}{n^2} P_{v_1 \rightarrow v'_1}^{v_2 \rightarrow v'_2} + \frac{n_{v'_1} n_{v'_2}}{n^2} P_{v'_1 \rightarrow v_1}^{v'_2 \rightarrow v_2} \right) \epsilon_{v_1}. \quad (53)$$

Equation (52) for the master equation is convenient because it is now written in terms of the fractional population.

If all the parameters appearing in the right-hand side [Eq. (52)] are defined for a specified position denoted by x_i (see Appendix), then Eq. (52) may be integrated numerically and the vibrational energy may be calculated. This set of equations is coupled to the macroscopic fluid equations since the right-hand side of Eq. (52) is a function of u , n , and T . If Eqs. (3) and (8) are differentiated with respect to x , and combined with Eqs. (1), (2), and (7), one can show

$$\frac{\partial u}{\partial x} = -\frac{u}{(1-M^2)} \left(\frac{1}{A} \frac{dA}{dx} + \frac{2}{7RT} \frac{\partial \bar{E}_{\text{vib}}}{\partial x} \right), \quad (54)$$

where M is the frozen Mach number given by

$$M = u / \sqrt{7RT/5}. \quad (55)$$

The system of differential equations given, respectively, by Eqs. (52)–(54) may be integrated if the flow parameters are specified at x_i . In this paper, in order to avoid both the calculation of the nonequilibrium mass flow, and the singularity occurring at $M=1$ in Eq. (54), we assume that the gas is in equilibrium from the reservoir to the cross sectional area for which $M \approx 1$. This approximation may be justified, since the vibrational relaxation time is very fast in comparison with the rate of expansion until the singularity $M=1$. The calculation of the equilibrium mass flow and of the flow parameters at x_i where $M \approx 1$ is presented in the Appendix. Equations (52)–(54) are integrated numerically. Thus the vibrational energy and the velocity are defined at each step. The temperature and the mass density are, respectively, calculated from the enthalpy and mass conservation. The pressure is deduced from the equation of state. The numerical integration is performed by using the semi-implicit extrapolation method of Bader and Deuffhard⁴⁹ which is for stiff differential equations.⁵⁰ The Jacobi matrix of derivatives, which is required for the numerical integration, is calculated numerically with the Ridders method.^{50,51}

B. With reaction

The master equation in Eq. (13) is transformed to calculate the spatial evolution of the fractional population of each vibrational level. The fractional population is expressed as a function of the vibrational distribution function,

$$Y_{v_1} = \frac{2n_{v_1}}{2n + n_O}, \quad (56)$$

where $M_{O_2} = 2M_O$ has been used. The fractional population Y_v is normalized to Y_{O_2} . The continuity equation is obtained by summing Eq. (13) over v_1 , and we have

$$\frac{\partial (2n + n_O) uA}{\partial x} = 0. \quad (57)$$

With Eqs. (56) and (57), one can show

$$\frac{\partial Y_{v_1}}{\partial x} = \frac{2}{(2n + n_O) Au} \frac{\partial n_{v_1} uA}{\partial x}. \quad (58)$$

Since $[(2n + n_O) Au]$ is independent of x , we can write the master equation analogous to Eq. (52) in the following form:

$$u \frac{\partial Y_{v_1}}{\partial x} = \frac{Z_{11}}{Y_{O_2}} \left[\sum_{v_2, v'_1, v'_2} -Y_{v_1} Y_{v_2} P_{v_1 \rightarrow v'_1}^{v_2 \rightarrow v'_2} + Y_{v'_1} Y_{v'_2} P_{v'_1 \rightarrow v_1}^{v'_2 \rightarrow v_2} + \sum_{v_2, v'_2} -Y_{v_1} Y_{v_2} P_{v_1 \rightarrow d}^{v_2 \rightarrow v'_2} + 2Y_{O_2}^2 Y_{v'_2} (2n + n_O) P_{d \rightarrow v_1}^{v'_2 \rightarrow v_2} \right] + Z_{12} \left[\sum_{v'_1} -Y_{v_1} P_{v_1 \rightarrow v'_1} + Y_{v'_1} P_{v'_1 \rightarrow v_1} - Y_{v_1} P_{v_1 \rightarrow d} + 2Y_{O_2}^2 (2n + n_O) P_{d \rightarrow v_1} \right]. \quad (59)$$

If Eqs. (3) and (8) are differentiated with respect to x , and combined with Eqs. (1), (2), and (8), one can show

$$\frac{\partial u}{\partial x} = -\frac{u}{P(1-M^2)} \left\{ \frac{P}{A} \frac{dA}{dx} + \frac{2\rho(1+Y_O)}{(7+3Y_O)} \left[\left(\frac{3}{2} RT - \bar{E}_{\text{vib}} + h^0 \right) \frac{\partial Y_O}{\partial x} + (1-Y_O) \frac{\partial \bar{E}_{\text{vib}}}{\partial x} \right] - \rho RT \frac{\partial Y_O}{\partial x} \right\}, \quad (60)$$

where M is the frozen Mach number given by

$$M = u \sqrt{5 + Y_O} / \sqrt{(7 + 3Y_O)(1 + Y_O)RT}. \quad (61)$$

The vibrational energy given by Eq. (6) is rewritten as a function of the fractional population,

$$\bar{E}_{\text{vib}} = \frac{1}{M_{O_2} Y_{O_2}} \sum_v Y_v \epsilon_v. \quad (62)$$

Equation (62) is differentiated so that $\partial \bar{E}_{\text{vib}} / \partial x$ given by

$$\frac{\partial \bar{E}_{\text{vib}}}{\partial x} = \frac{1}{Y_{O_2} M_{O_2}} \frac{\partial \sum Y_v \epsilon_v}{\partial x} - \frac{\bar{E}_{\text{vib}}}{Y_{O_2}} \frac{\partial Y_{O_2}}{\partial x}, \quad (63)$$

can be substituted into Eq. (60). The numerical integration of Eqs. (59) and (60) requires initial conditions. As in Sec. IV A, we avoid the calculation of the nonequilibrium mass flow and the singularity occurring at $M=1$ by assuming that the gas is in equilibrium from the reservoir to the cross sectional area where $M \approx 1$. The calculation of the initial conditions at x_i where the frozen Mach number is close to unity are presented in the Appendix. The numerical integration is performed similarly to Sec. IV A.

V. COMPARISON WITH TREANOR AND LANDAU–TELLER MODELS FOR VIBRATIONAL RELAXATION

The vibrational distribution obtained from the master equation is compared with the distribution calculated with the model of Treanor *et al.*²⁵ In this model, the $T-V$ and $V-V$ energy exchanges governing the vibrational distributions are assumed to proceed with two different time scales, that is $\tau_{V-V} \ll \tau_{T-V}$. As a result, a quasisteady distribution function is maintained by the $V-V$ energy exchanges and the vibrational distribution is assumed to be of the form,²⁵

$$n_v / n = \exp \left(-\frac{\epsilon_v}{kT} + vK(x) \right) /$$

$$\sum_v \exp \left[-\frac{\epsilon_v}{kT} + vK(x) \right], \quad (64)$$

parametrized by the parameter $K(x)$ which describes the extent of the nonequilibrium. When $K=0$, the gas is in equilibrium. This model is completely specified when $K(x)$ is known. We provide here a brief outline of the procedure to calculate $K(x)$. The derivative $\partial K(x) / \partial x$ can be obtained by differentiating the averaged quantum number \bar{V} given by

$$n\bar{V} = \sum_v n_v v. \quad (65)$$

The relaxation equation for this model is given by

$$\frac{\partial \bar{V}}{\partial x} = \frac{\{\exp[-K(x)] - 1\}}{u} Z_{11} \sum_{v_1, v_2} P_{v_1 \rightarrow v_1 - 1}^{v_2 \rightarrow v_2} n_{v_1} / n. \quad (66)$$

Equations (64) and (65) are used to calculate $(\partial \bar{V} / \partial x) = (\partial \bar{V} / \partial T)(\partial T / \partial x) + (\partial \bar{V} / \partial K)(\partial K / \partial x)$. This differential equation is combined appropriately with the conservation equations and the equation of state to give a set of seven equations of the form $\partial M_n / \partial x = f_n(u, T, \bar{E}_{\text{vib}}, P, \rho, K, A)$ where M_n is, respectively, equal to $u, T, \bar{E}_{\text{vib}}, P, \rho, K, A$. This system is numerically integrated. In this way, the vibrational distribution function may be calculated as a function of x .

The separation of time scales between τ_{T-V} and τ_{V-V} was also utilized to show that for a harmonic oscillator model, the population distribution is a Boltzmann distribution function¹ characterized by a vibrational temperature (T_{vib}),

$$n_v / n = \exp \left(-\frac{\epsilon_v}{kT_{\text{vib}}} \right) / \sum_v \exp \left(-\frac{\epsilon_v}{kT_{\text{vib}}} \right). \quad (67)$$

In this model, the de-excitation probabilities are proportional to the vibrational quantum number of the molecule,

$$P_{v_1 \rightarrow v_1 + 1}^{v_2 \rightarrow v_2} = (v_1 + 1) P_{1 \rightarrow 0}^{v_2 \rightarrow v_2}, \quad (68)$$

and

$$P_{v_1 \rightarrow v_1 + 1}^{v_2 \rightarrow v_2 - 1} = v_2 (v_1 + 1) P_{0 \rightarrow 1}^{1 \rightarrow 0}. \quad (69)$$

Equations (53), (67)–(69) are combined to give the well-known Landau–Teller equation,

$$\frac{\partial E_{\text{vib}}}{\partial x} = (E_{\text{vib}}^{\text{eq}}(T) - E_{\text{vib}}) Z_{11} P_{1 \rightarrow 0}^{v_2 \rightarrow v_2} \left[1 - \exp \left(-\frac{\hbar \omega}{kT} \right) \right] / u, \quad (70)$$

where $E_{\text{vib}}^{\text{eq}}(T)$ is the equilibrium value of E_{vib} . Equations (70) and (54) are solved numerically. At each step, the calculation of E_{vib} enables one to calculate T_{vib} and to determine n_v/n from Eq. (67).

VI. RESULTS AND DISCUSSION

A. No reaction

The computation is performed for a nozzle with cross-sectional area distribution similar to that defined in the introduction. The reservoir temperature is 2400 K, the pressure is 100 atm, and the atomic mass fraction is smaller than 10^{-4} . As a result, the reactive processes are neglected. In addition, the fractional populations for the high vibrational levels are small ($n_{18}/n < 10^{-8}$). The computation is performed for the first 18 vibrational levels, since the contribution of the higher vibrational levels on the vibrational energy and on the macroscopic parameters is negligible.

In Fig. 8, we show the results of the calculations of vibrational relaxation without reaction, and give n_v/n vs $A(x)/A_t$ for $v=0, 1, 5, 10, 17$. The four curves in each graph correspond to (a) $T-V$ and $V-V$ energy exchanges included in Eq. (52), (b) $V-V$ energy exchanges neglected, (c) the model by Treanor *et al.*,²⁵ and (d) the Landau–Teller model. The relaxation zone may be divided in two regions. The first one is located just downstream of the throat until the cross sectional area $A(x)/A_t \approx 4$, where the vibrational relaxation is dominated by the $T-V$ energy exchanges [Figs. 8(A)–(E)]. In this zone, the translational–rotational temperature decreases quickly with increasing $A(x)$ and, consequently, the transitions involving $T-V$ energy decreases strongly with increasing $A(x)$. The second region is located beyond $A(x)/A_t \approx 4$ where the vibrational relaxation is governed by the $V-V$ energy exchanges.

In Fig. 8(A), the fractional population n_0/n for the ground state increases strongly from the throat until the cross-sectional area $A(x) \approx 4A_t$. Beyond this cross-sectional area, n_0/n is frozen when it is determined from a Boltzmann distribution, and when the $V-V$ exchanges are neglected. For cross sectional areas $A(x)/A_t \geq 4$, n_0/n increases more slowly when the $V-V$ exchanges are taken into account in Eq. (52). Also, n_0/n increases slightly more quickly with the model of Marrone *et al.* than when the $V-V$ exchanges are included in Eq. (51) because the $V-V$ energy exchanges are overestimated. In Fig. 8(B), n_1/n decreases monotonically for the three of the four-cases studied [curves (a)–(c)] for which $V-V$ energy exchanges are included, whereas n_1/n is frozen for $A(x)/A_t \geq 4$ when $V-V$ energy exchanges are neglected, curve (d). A similar behavior is observed for n_2/n .

For the remaining vibrational levels ($v > 2$), the effect of the $V-V$ energy exchanges is opposite to $T-V$ energy exchanges. After a strong de-excitation zone due to the $T-V$ de-excitation processes ($A(x)/A_t \leq 4$), the vibrational distribution function increases slowly when the cross sectional area increases. In Figs. 8(A)–(D), the effect of the $V-V$ exchanges is stronger when the vibrational level increases. In Fig. 9, we show the fractional population n_v/n versus v for a cross sectional area $A(x)/A_t = 23.1$. The vibrational distribu-

tion function calculated with the model of Marone *et al.* [curve (c)] is very close to the one determined from the master equation [curve (a)]. When the effect of the $V-V$ energy exchanges is neglected [curve (b)], the vibrational distribution function is close to those determined from the Boltzmann distribution [curve (d)] characterized by T_{vib} . The comparison between curves (a) and (b) shows that the $V-V$ energy exchanges create a distortion of the vibrational distribution when $A(x)/A_t \geq 4$ and that the effect of the $V-V$ exchanges increases with the vibrational level. However, the vibrational energy remains frozen in the zone where the $V-V$ exchanges have a strong influence on the distribution function, since the $V-V$ exchanges have a strong influence on vibrational levels for which the populations are small. Moreover, when the effect of the $V-V$ exchanges is neglected in the master equation, at a given cross sectional area, the vibrational energy is slightly higher than when the $V-V$ exchanges are included. This result is confirmed, when one calculates the vibrational energy with the population distribution function, obtained with the model of Marrone *et al.* where the influence of the $V-V$ exchanges is overestimated. When the cross sectional area increases, the $V-V$ energy exchanges reduce the average vibrational energy and increase the translational–rotational temperature (not shown).

B. With reaction

When the reservoir temperature is $T_r = 5000$ K and the pressure is $P_r = 90$ atm, the gas is partially dissociated and $Y_{\text{O}_2,r} = 0.6545$. Consequently, the reactive processes are included in the master equation, and the contribution of all the vibrational levels on the vibrational energy and on the reaction rate coefficient is significant. For this case, the computation is performed with 37 vibrational levels.

We first compare the vibrational distribution function calculated when the reactive processes are accounted for in the master equation with that obtained when they are neglected. Then, we compare the vibrational distribution function and the departure of the rate coefficients from their equilibrium values calculated with the model of KH to those calculated with the model of RB. The different values of l presented in Sec. III A are employed, and the influence of l on the deviation of the macroscopic forward rate coefficients $k_{f,11}$ and $k_{f,12}$ from their equilibrium values is discussed. The contribution of each vibrational level to the macroscopic forward rate coefficient is also calculated for different cross-sectional areas determined from numerical integration of Eq. (59) as discussed in Sec. IV B.

In Fig. 10, the fractional population for the ground state Y_0 is plotted as a function of $A(x)/A_t$. The calculation is performed with both the model of KH and by neglecting the reactive processes in Eq. (59). The solid curve is with reaction and the dashed curve is without reaction. The fractional population of the ground state Y_0 increases with increasing x . The temperature drops rapidly with increasing cross-sectional area of the nozzle, and the reactive processes proceed mainly through recombination. Consequently, when the reactive processes are not included in the master equation,

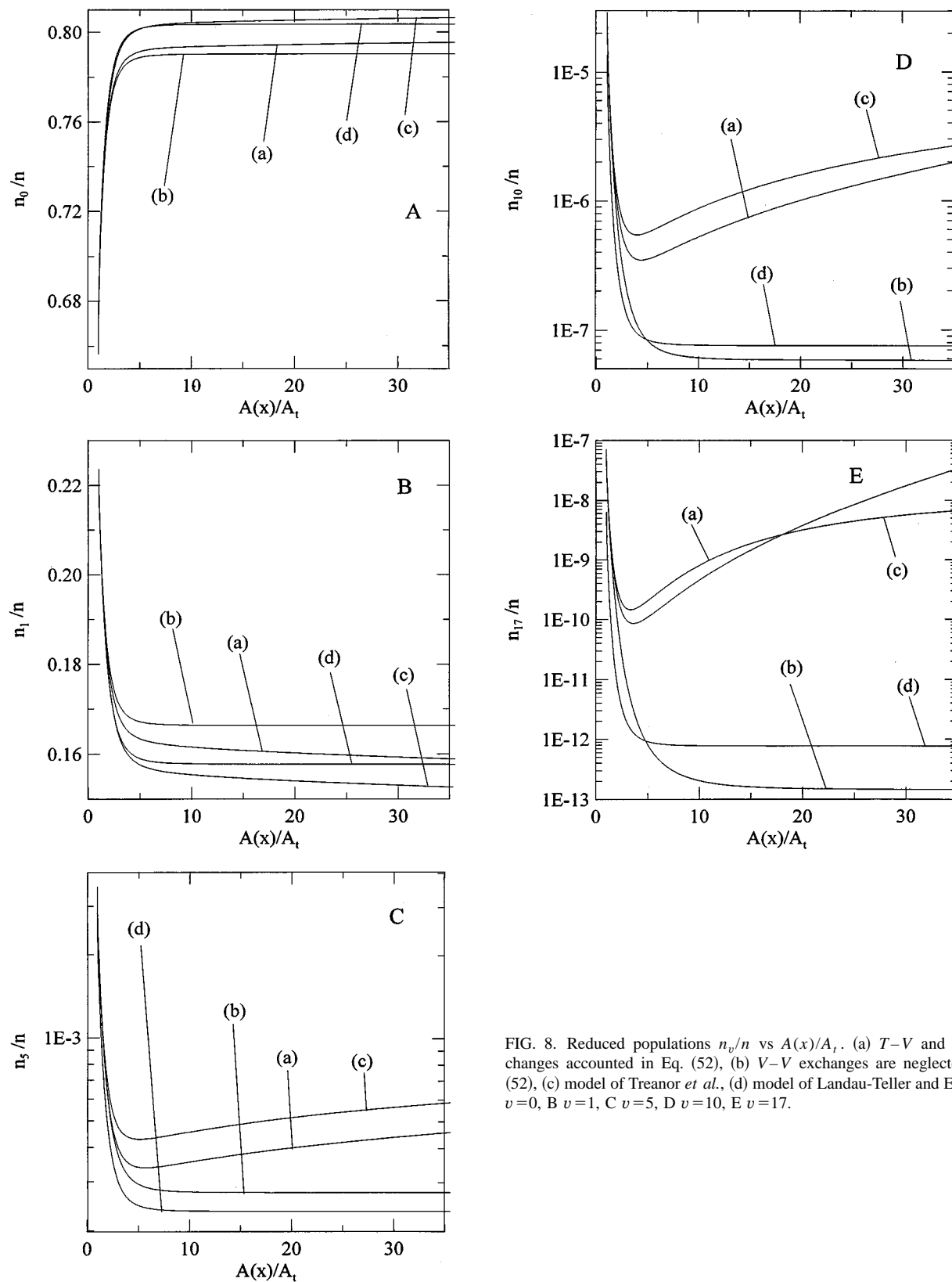


FIG. 8. Reduced populations n_v/n vs $A(x)/A_t$. (a) $T-V$ and $V-V$ exchanges accounted in Eq. (52), (b) $V-V$ exchanges are neglected in Eq. (52), (c) model of Treanor *et al.*, (d) model of Landau-Teller and Eq. (67). A $v=0$, B $v=1$, C $v=5$, D $v=10$, E $v=17$.

the fractional population distribution function is smaller than that obtained when the reactive processes are accounted for. As is clear from Fig. 10, the reactive processes have a strong influence on the fractional population Y_0 . In Fig. 11, the fac-

tional population Y_v for $v=1,2,3$ is shown versus $A(x)/A_t$. Y_v increases strongly behind the throat of the nozzle, due to the reactive processes; but the influence of the reactive processes decreases with increasing vibrational levels. Conse-

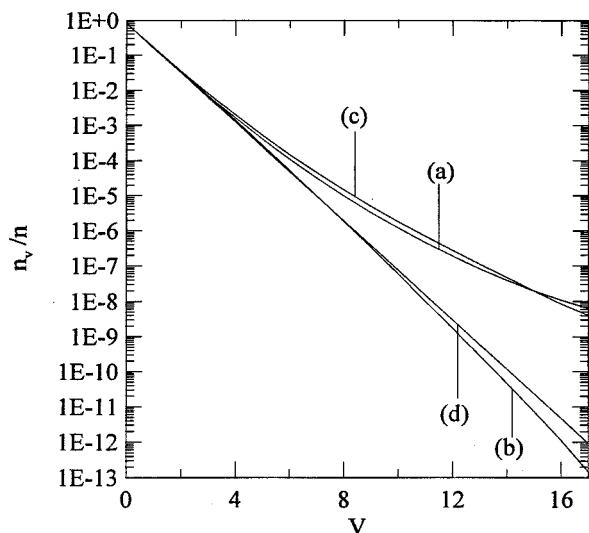


FIG. 9. Fractional populations n_v/n vs v . $A(x)/A_t=23.1$. (a) $T-V$ and $V-V$ exchanges accounted in Eq. (52), (b) $V-V$ exchanges are neglected in Eq. (52), (c) Treanor *et al.*, (d) Landau-Teller and Eq. (67).

quently, the first vibrational levels have a strong influence on the profile of Y_{O_2} .

In Fig. 12, we compare the variation of Y_v for $v=1,2,3$ calculated with the model of KH (solid curve) to those calculated with the model of RB (dashed curve). The trend for the vibrational distribution is the same with both models. As is clear from Fig. 6 and 7, the reactive cross sections for $v \leq 10$ calculated with the model of KH are larger than those calculated with the model of RB for O_2-O and O_2-O_2 collisions. Consequently, the backward probabilities for $v \leq 10$ calculated with the model of KH are also larger than those calculated with the model of RB. As a result, Y_v for $v=1,2,3$ calculated with the model of KH are larger than those calculated, with the model of RB with increasing $A(x)/A_t$.

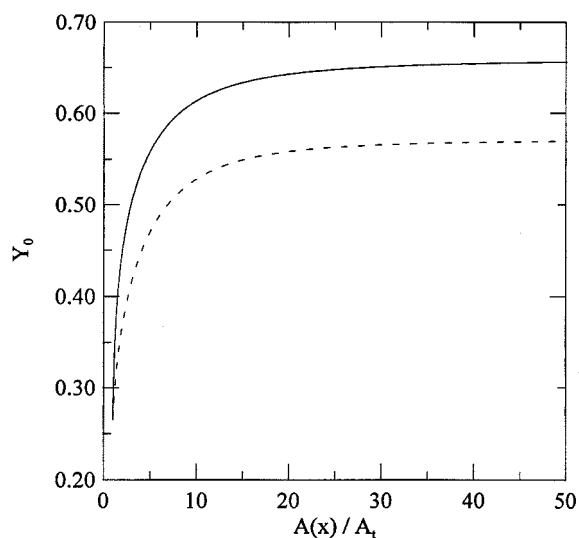


FIG. 10. Fractional population Y_0 vs $A(x)/A_t$. (—) with reaction, (---) without reaction.

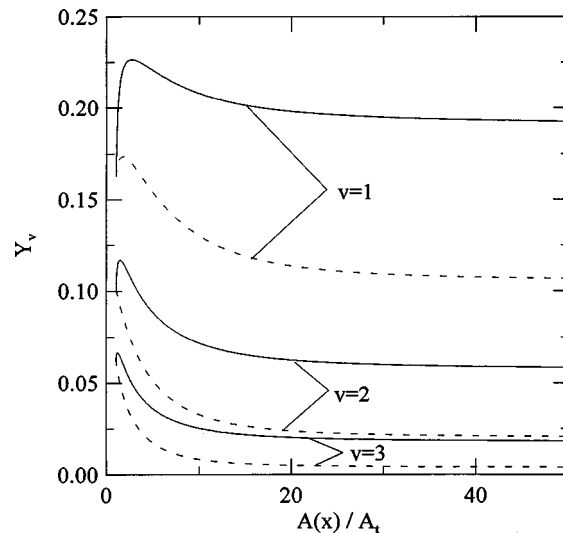


FIG. 11. Fractional populations Y_1 , Y_2 , and Y_3 vs $A(x)/A_t$. (—) with reaction, (---) without reaction.

In Fig. 13, we show the variation of the fractional populations Y_v for $v=30-35$ versus $A(x)/A_t$. Just behind the throat, the fractional populations of the high vibrational levels decrease quickly due to vibrational de-excitation. As the rate of expansion increases, the variation of the fractional populations becomes very slow.

In Fig. 14, we show the variation of the fractional population of the topmost vibrational level Y_{36} versus $A(x)/A_t$. The solid line is with reaction and the dashed line without reaction. The main variation of Y_{36} is due to the vibrational relaxation and not to reactive processes. Y_{36} decreases with increasing x to populate the other fractional populations when the reactive processes are included or not in the master equation.

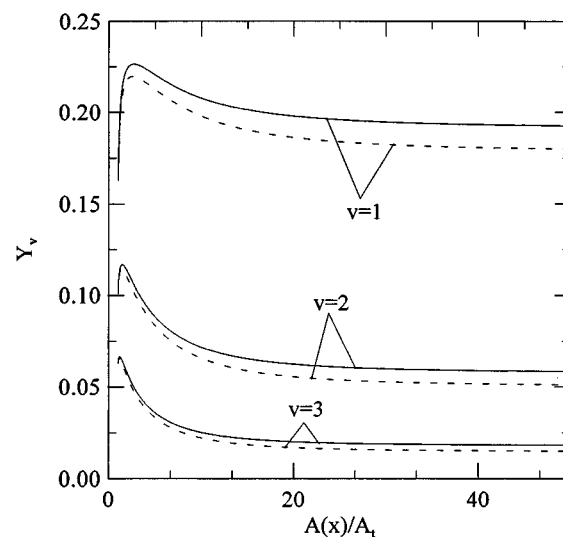


FIG. 12. Fractional populations Y_1 , Y_2 , and Y_3 vs $A(x)/A_t$. (—) with the model of KH and normalization A , (---) with the model of RB and normalization C .

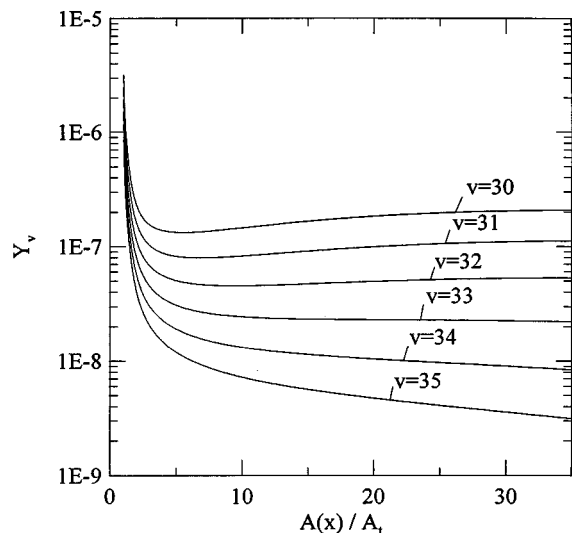


FIG. 13. Fractional populations Y_v for $v=30-35$ vs $A(x)/A_t$ with the model of KH and normalization A.

The mass fraction Y_{O_2} in Fig. 15 increases strongly behind the throat because of the strong variation of the fractional populations Y_0, Y_1, Y_2 and Y_3 . The contribution of the fractional population of the other vibrational levels on Y_{O_2} is less significant. According to the fractional populations distribution plotted in Fig. 12, Y_{O_2} calculated with the model of KH is larger than Y_{O_2} calculated with the model of RB with increasing x .

The different values of l employed in Sec. III are used in order to assess the influence of the vibrational relaxation time on the macroscopic reaction rates and on the deviations F_1 and F_2 given in Eqs. (34) and (35). In Figs. 2 and 3, the vibrational cross sections $\sigma_{1 \rightarrow 0}$ for, respectively, O_2-O and O_2-O_2 increase when l decreases. Consequently, from Eq. (37), the vibrational relaxation time decreases with l increas-

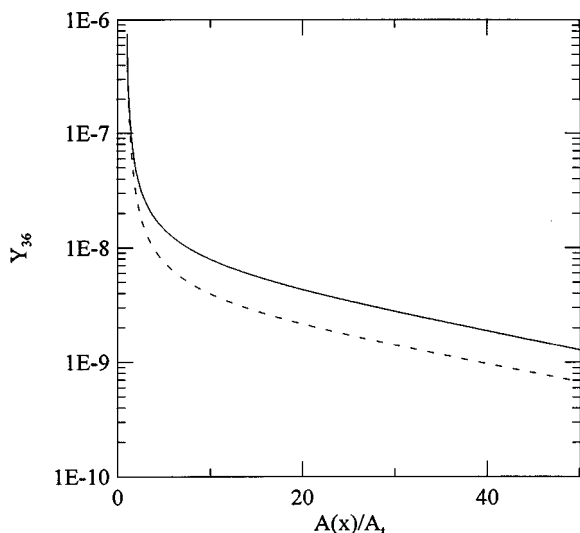


FIG. 14. Fractional population Y_{36} vs $A(x)/A_t$. (—) with reaction, (---) without reaction.

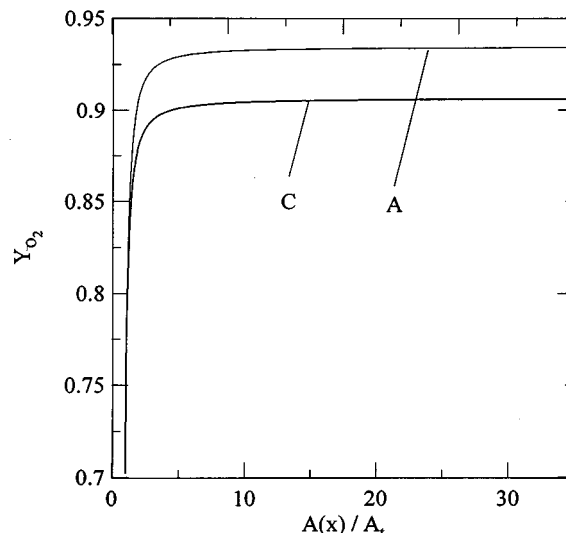


FIG. 15. Mass fraction Y_{O_2} vs $A(x)/A_t$. (A) with the model of KH and normalization A, (C) with the model of KH and normalization C.

ing. F_1 and F_2 decrease with decreasing the vibrational relaxation time because both the vibrational distribution function, and the forward macroscopic rate coefficients are closer to their equilibrium values. For $A(x)/A_t=30$, the deviations calculated with $l=0.3508 \text{ \AA}$ are equal to $F_1=8.07 \times 10^{12}$ and $F_2=1.97 \times 10^{12}$ whereas those calculated with $l=0.256 \text{ \AA}$ are equal to $F_1=7.71 \times 10^{12}$ and to $F_2=1.88 \times 10^{12}$ for O_2-O and O_2-O_2 collisions, respectively. The influence of l on the deviation increases with increasing the cross sectional area. The molecular mass fraction calculated by setting $l=0.256 \text{ \AA}$ is slightly larger than that calculated with $l=0.3508 \text{ \AA}$, because the macroscopic forward reaction rate decreases with increasing the vibrational relaxation time, which increases the rate of recombination. The different values of l for O_2-O collisions presented in Sec. IV were also employed. However, the influence of l on the deviations F_1 and F_2 is not significant. Even though $\sigma_{1 \rightarrow 0}$ is of the order of $\sigma_{12,e}$ at 5000 K, the atomic mass fraction is weak compared to the molecular one, and O_2-O collisions have small effects on the vibrational relaxation time.

In Fig. 16, the deviations F_1 (dashed line) and F_2 (solid line) calculated with the model of KH (curves A) and with the model of RB (curves C) increase with increasing the cross sectional area. F_1 and F_2 become of the order of 10^{13} for $A(x)/A_t=30$ when they are calculated with the model of KH and are of the order of 10^{15} when they are calculated with the model of RB. The deviations F_1 and F_2 are large for two reasons. First, because the temperature drops rapidly, the vibrational relaxation times increases considerably and the vibrational distribution function is far from its equilibrium value. Second, the velocity increases on a short time scale, which reduces the spatial variation of the vibrational distribution function. The vibrational relaxation and the reactive processes affect the vibrational energy, and the molecular mass fraction for cross section areas $A(x)/A_t \lesssim 10$. Beyond

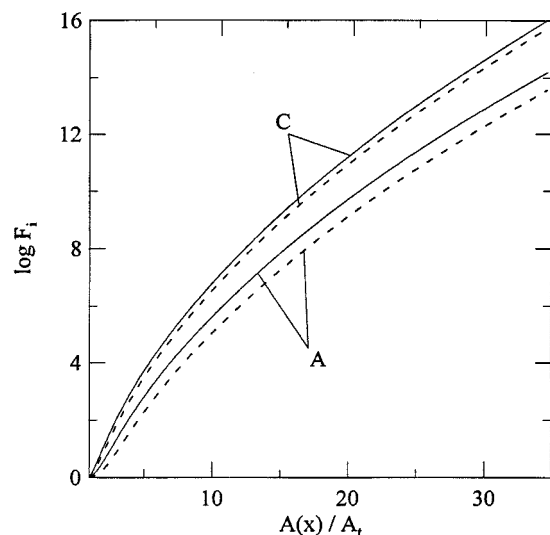


FIG. 16. Factor F_1 versus $A(x)/A_t$. (---) $i=1$ for O_2-O_2 collisions, (—) $i=2$ for O_2-O collisions. (A) model of KH model and normalization A. (C) model of RB and normalization C.

$A(x)/A_t \approx 10$, the vibrational energy and the molecular mass fraction are frozen.

In order to show the influence of the vibrational distribution function on F_1 , we calculate F_1 by assuming a Boltzmann distribution characterized by T_{vib} . If Eqs. (42) and (48) are combined, one can show

$$k_{f,11}(v \rightarrow d, T) = k_{f,11}^{\text{eq}} \frac{Q(T)}{Q(-U_{11})} \exp\left[\frac{\epsilon_v}{k} (1/U_{11} + 1/T)\right], \quad (71)$$

where $Q(T)$ is the partition function and $\lambda_{11} = D/kU_{11}$ has been used. With Eqs. (22), (67) and (71), one can show

$$F_1 = \frac{Q(T_f)Q(T)}{Q(T_{\text{vib}})Q(-U_{11})}, \quad (72)$$

where $1/T_f = 1/T_{\text{vib}} - 1/U_{11} - 1/T$. In Eq. (72), F_1 is the same as that proposed by Marrone and Treanor.²⁹ In Eq. (71), we use the value of λ_{11} calculated with normalization A in Sec. III B. We also calculate, F_1 by assuming a Treanor *et al.* vibrational distribution function given by Eq. (64). The parameter $K(x)$ is calculated from the averaged vibrational energy, and T_{vib} in Eq. (72) is determined similarly. In Fig. 17, we show F_1 versus $A(x)/A_t$ calculated with the vibrational distribution function determined from the master equation [curve (a)], which is larger than F_1 calculated by assuming a Boltzmann distribution [Eq. (72)] [curve (b)], and larger than F_1 calculated with a Treanor *et al.* distribution [Eq. (64)]. The deviation F_1 are smaller in curves (b) and (c) than in curve (a) because the populations of the high vibrational levels calculated from Eqs. (64) and (67), are smaller than those calculated from the master equation.

In Fig. 18, we plot the vibrational distribution function calculated from the master equation [Eq. (59)] in the form $\log[(n_v/n)\exp(\epsilon_v/kT)]$ versus v for different cross-sectional areas [curves (a)–(e)]. If Eq. (64) is a good approximation, we expect a linear variation with v , with slope equal to $K(x)$.

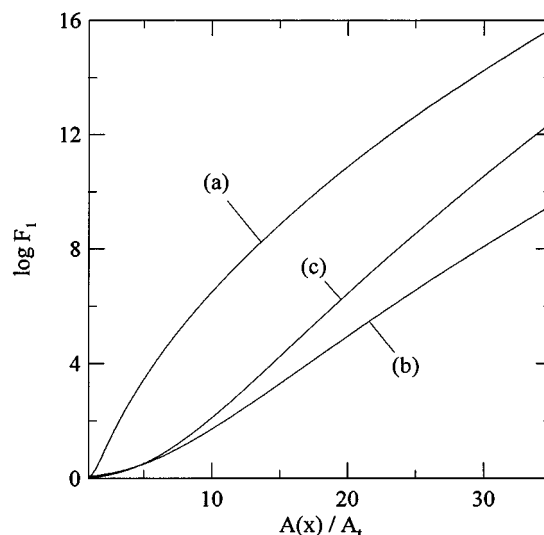


FIG. 17. Factor F_1 vs $A(x)/A_t$. The vibrational distribution function is determined (a) from Eq. (59), (b) from Eq. (67), (c) from Eq. (64).

Close to the throat [curve (a)], the nonequilibrium effects are weak, the curve is linear, and $K(x)$ is independent of v . With increasing the cross sectional area, the nonequilibrium effects are larger and the parameter K depends on v . Figure 18 shows that for $v=0-10$, there is a linear portion for which a $K(x)$ can be calculated from the slope of curves (b)–(e). For $A(x)/A_t=1.18$, [curve (a)] and 27.34 [curve (e)], we obtain $K=0.179 \times 10^{-2}$ and $K=0.71$, respectively. We have also calculated K by equating the averaged vibrational energy determined from the Treanor *et al.* distribution function to that determined from the vibrational distribution obtained with the master equation. We find that for $A(x)/A_t=1.18$ and 27.34, $K=0.163 \times 10^{-2}$ and 0.79, respectively.

The macroscopic forward reaction rate is equal to the sum of all individual dissociative transitions. The contribu-

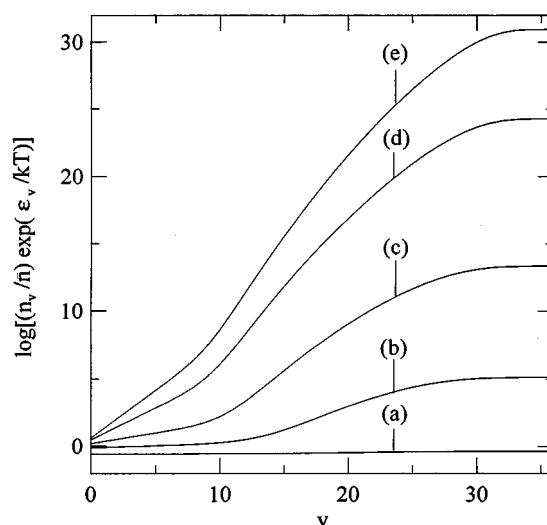


FIG. 18. $\log[(n_v/n)\exp(\epsilon_v/kT)]$ vs v . (a) $A(x)/A_t=1.18$, (b) $A(x)/A_t=3.57$, (c) $A(x)/A_t=8.73$, (d) $A(x)/A_t=19.06$, (e) $A(x)/A_t=27.34$.

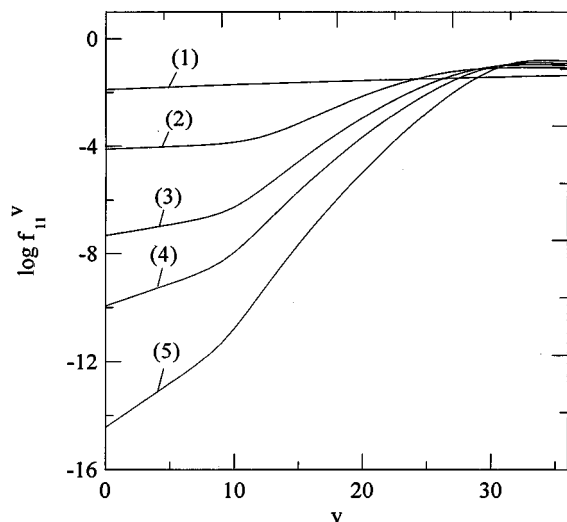


FIG. 19. $\log f_{11}^v$ vs $A(x)/A_t$. (1) $A(x)/A_t=1.02$, (2) $A(x)/A_t=4.7$, (3) $A(x)/A_t=10.6$, (4) $A(x)/A_t=16.8$, (5) $A(x)/A_t=30.72$.

tion of each individual transition on the forward macroscopic rate coefficient is shown with the coefficient,

$$f_{11}^v = (n_v/n) k_{f,11}(v \rightarrow d, T) / k_{f,11} \\ = \overline{n_v \sigma_{v \rightarrow d}} / \sum_v \overline{n_v \sigma_{v \rightarrow d}}. \quad (73)$$

In Fig. 19, the fraction f_{11}^v is plotted against the vibrational level v for different $A(x)/A_t$ [curves (1)–(5)]. It can be seen that the contribution to $k_{f,11}$ is almost equal, whatever is the vibrational level when the vibrational distribution function is closed to equilibrium ($A(x)/A_t \approx 1$). Nevertheless, in Fig. 17, the contribution of the high vibrational levels [curves (2)–(5)] increases quickly with increasing $A(x)/A_t$ for two reasons. First, when the temperature drops, the reactive cross section of the high vibrational level remains of the order of magnitude of the hard sphere cross section, whereas those of the other vibrational levels decreases quickly. Second, for $A(x)/A_t \lesssim 5$, the vibrational distribution function is almost frozen and the populations of the high vibrational level are higher than that calculated when the flow is in equilibrium. The function f_{12}^v which characterizes O_2 –O collisions has a similar trend.

In this paper, the nonequilibrium phenomena differ from those of a previous paper¹⁸ where the nonequilibrium effects are generated by a shock wave. In this study, the gas is initially in equilibrium, and the nonequilibrium effects are produced by the expansion. In the reservoir, since the vibrational distribution function is equal to its equilibrium value, the forward rate coefficients are equal to their equilibrium values. As the rate of expansion increases, the vibrational distribution function is perturbed by both vibrational energy exchanges, mainly through de-excitations and reactive processes, mainly through recombination. Nevertheless, the vibrational distribution function remains far from its equilibrium value, and the forward rate coefficients become much bigger than their equilibrium values. On the other hand, in

our previous study, just behind the shock wave, the gas is in nonequilibrium and the forward rate coefficients are negligible compared to their equilibrium values because only the fractional population for the ground state is significant. However, as the distance behind the shock wave increases, the vibrational distribution function is perturbed by both vibrational energy exchanges, mainly through excitations and reactive processes, mainly through dissociation. As the gas moves toward an equilibrium value, the forward rate coefficients approach their equilibrium value.

VII. SUMMARY

In this article, we have calculated the increase in the forward rates of O_2 – O_2 and O_2 –O reactions from their equilibrium values for the hypersonic expansion of O_2 through a nozzle. The increase in the forward rates is due to the perturbation of the vibrational distribution function by T – V , V – V , and reactive processes. The vibrational distribution function is calculated from a numerical solution of a master equation, which is coupled to the conservation equations. The deviations of the reaction rates from their equilibrium values are strong, and increase, with increasing the cross sectional area. In addition, our calculations show that the contribution to the forward reaction rates comes from all the vibrational levels, when the gas is located close to the throat, and from the highest vibrational levels when the gas is far from the throat.

ACKNOWLEDGMENTS

This research is supported by a grant from the Natural and Engineering Research Council of Canada, and NATO Grant No. CRG931332. We are grateful to Dr. David Zeitoun for reading the manuscript prior to publication and for several helpful comments.

APPENDIX: DETERMINATION OF THE INITIAL CONDITIONS FOR THE NUMERICAL INTEGRATION

The equilibrium mass flow is determined at the throat where the position is x_t and $(dA/dx)_{x_t} = 0$. In order to remove the singularities occurring at $M=1$ in Eqs. (54) or (60), and to calculate the initial conditions necessary to integrate Eqs. (52)–(54) or (59) and (60), we assume that the flow is in equilibrium until the position where the frozen Mach number is slightly greater than unity.

From the equation of motion, Eq. (2), we can show

$$\frac{\partial P}{\partial \rho} \frac{\partial \rho}{\rho} = -u \partial u. \quad (A1)$$

The logarithmic derivation of the mass conservation gives

$$\frac{\partial \rho}{\rho} + \frac{\partial A}{A} + \frac{\partial u}{u} = 0. \quad (A2)$$

If $(\partial \rho / \rho)$ from Eq. (A2) is substitute into (A1), we find the fundamental relation for one-dimensional compressible flow,

$$\frac{1}{A} \frac{dA}{dx} = -\frac{1}{u} \frac{\partial u}{\partial x} \left(1 - \frac{u^2}{(\partial P / \partial \rho)_s} \right). \quad (\text{A3})$$

The subscript “s” indicates that the entropy is constant.

1. In the absence of reaction

The final desired result involves explicit evaluation of the sound speed $a_{\text{eq}}^2 = (\partial P / \partial \rho)_s$ for this molecular gas at equilibrium. If the ideal equation of state is differentiated with respect to x , then

$$\frac{(\partial P / \partial x)}{(\partial \rho / \partial x)} = RT \left(1 + \frac{\rho}{T} \frac{(\partial T / \partial x)}{(\partial \rho / \partial x)} \right). \quad (\text{A4})$$

The temperature is obtained by differentiating the enthalpy equation, $7/2 RT + \bar{E}_{\text{vib}}^{\text{eq}} + u^2/2 = h_r$, Eq. (3),

$$u \frac{\partial u}{\partial x} + \frac{7}{2} R \frac{\partial T}{\partial x} + \frac{\partial \bar{E}_{\text{vib}}^{\text{eq}}}{\partial T} \frac{\partial T}{\partial x} = 0. \quad (\text{A5})$$

The term in $u(\partial u / \partial x)$ in Eq. (A5) is replaced by $-1/\rho(\partial P / \partial x)$ with use of Eq. (2), and the result for $(\partial P / \partial x)$ given by Eq. (A4) is subsequently used. The resulting equation is solved for $(\partial T / \partial x)$ to give

$$\frac{\partial T}{\partial x} = \frac{2RT(\partial \rho / \partial x)}{\rho[5 + 2C_{\text{vib}}(T)]}, \quad (\text{A6})$$

where $C_{\text{vib}}(T) = (\partial \bar{E}_{\text{vib}}^{\text{eq}} / \partial T)$. With the substitution of Eq. (A6) into Eq. (A4), we have the final desired result

$$\left(\frac{\partial P}{\partial \rho} \right)_s = \left(\frac{7R + 2C_{\text{vib}}(T)}{5R + 2C_{\text{vib}}(T)} \right) RT. \quad (\text{A7})$$

In order to determine the temperature at the throat, we use the conservation of enthalpy. At the throat we have that $(dA/dx) = 0$. Consequently, from Eq. (A3), $u_t^2 = (\partial P / \partial \rho)_s$ and

$$h_r = \frac{7}{2} RT_t + \bar{E}_{\text{vib}}^{\text{eq}}(T_t) + \frac{u_t^2(T_t)}{2}, \quad (\text{A8})$$

where T_t is the temperature at the throat which is determined numerically from Eq. (A8). A supplementary macroscopic parameter must be defined in order to calculate the other parameters of the flow. The enthalpy, the momentum and the equation of state may be rearranged to give

$$\frac{\partial P}{\partial T} = \frac{P[7R + 2C_{\text{vib}}(T)]}{2RT}. \quad (\text{A9})$$

This equation can be numerically integrated with the Runge–Kutta method from the reservoir conditions as initial values (P_r and T_r) to the throat where the temperature is T_t . This integration enables one to calculate P_t and to deduce the mass flow

$$\dot{m}_{\text{eq}} = \rho_t u_t A_t. \quad (\text{A10})$$

In order to avoid the singularity occurring at $M=1$ in Eq. (54), the initial conditions necessary to integrate Eq. (52)–(54) are calculated at a position x_i , where the frozen Mach number is slightly greater than unity. For $M_i = (1 + \epsilon)$, from

Eq. (55), the velocity is $u_i^2 = (7RT_i/5)(1 + \epsilon)^2$. Thus, from the conservation of enthalpy, the temperature T_i may be numerically calculated. The pressure P_i is calculated by integrating Eq. (A9) from T_r and P_r to T_i . The density ρ_i is determined from the ideal gas equation of state, and A_i is given by Eq. (A10) from which the position x_i is determined from the nozzle profile, Fig. 1.

2. With reaction

The calculation of the equilibrium mass flow is more complicated, than in the absence of reaction because the atom mass fraction Y_O is an additional unknown appearing in the conservation equations. We follow the same procedure as in the absence of reaction. The final desired result involves explicit evaluation of the sound speed $a_{\text{eq}}^2 = (\partial P / \partial \rho)_s$ in Eq. (A3) for the gas mixture at equilibrium. If the ideal equation of state is differentiated with respect to x , then

$$\begin{aligned} \frac{(\partial P / \partial x)}{(\partial \rho / \partial x)} = RT \left(\frac{\rho}{T} (1 + Y_O) \frac{(\partial T / \partial x)}{(\partial \rho / \partial x)} + \rho \frac{(\partial Y_O / \partial x)}{(\partial \rho / \partial x)} \right. \\ \left. + (1 + Y_O) \right). \end{aligned} \quad (\text{A11})$$

The temperature is obtained by differentiating the enthalpy equation, Eq. (3),

$$\begin{aligned} u \frac{\partial u}{\partial x} + \left[\left(\frac{7}{2} + \frac{3}{2} Y_O \right) R + (1 - Y_O) C_{\text{vib}}(T) \right] \frac{\partial T}{\partial x} \\ - \left[\bar{E}_{\text{vib}}^{\text{eq}} - \frac{3}{2} RT - h^0 \right] \frac{\partial Y_O}{\partial x} = 0. \end{aligned} \quad (\text{A12})$$

The term in $u(\partial u / \partial x)$ in Eq. (A12) is replaced by $-1/\rho(\partial P / \partial x)$ with use of Eq. (2), and the result for $(\partial P / \partial x)$ given by Eq. (A11) is subsequently used. The resulting equation is solved for $(\partial T / \partial x)$ to give

$$\begin{aligned} \frac{\partial T}{\partial x} = \frac{1}{[R/2(5 + Y_O) + (1 - Y_O)C_{\text{vib}}(T)]} \\ \times \left[(\bar{E}_{\text{vib}}^{\text{eq}} - RT/2 - h^0) \frac{\partial Y_O}{\partial x} + \frac{RT(1 + Y_O)}{\rho} \frac{\partial \rho}{\partial x} \right]. \end{aligned} \quad (\text{A13})$$

In order to express $(\partial Y_O / \partial x)$ as a function of T , Y_O , ρ , $(\partial T / \partial x)$, $(\partial \rho / \partial x)$, we need a further relation. We employ the law of mass action. The equilibrium constant $K_c(T)$ for the reaction



where M is either O_2 or O and is given by

$$\begin{aligned} K_c(T) = \frac{[\text{O}]^2}{[\text{O}_2]} = \frac{4\rho Y_O^2}{\hat{M}_{\text{O}_2}(1 - Y_O)} \\ = \frac{K^{\text{eq}}}{N_A} = \exp \left[A_1 \left(\frac{T}{B} \right) + A_2 + A_3 \ln \left(\frac{B}{T} \right) \right] \end{aligned}$$

$$+A_4\left(\frac{B}{T}\right)+A_5\left(\frac{B}{T}\right)^2, \quad (\text{A15})$$

determined by experiment. $[O]$ and $[O_2]$ are, respectively, the equilibrium concentration in moles per unit volume of O and O_2 . K^{eq} is the equilibrium rate constant given by Eq. (31). The values of $B, A_1, A_2, A_3, A_4, A_5$ are given by Park.⁸ The term $(\partial Y_O/\partial x)$ in Eq. (A13) is obtained by differentiating Eq. (A15),

$$\frac{\partial Y_O}{\partial x} = \frac{Y_O(1-Y_O)}{(2-Y_O)} \left(\frac{1}{K_c(T)} \frac{\partial K_c(T)}{\partial x} - \frac{1}{\rho} \frac{\partial \rho}{\partial x} \right). \quad (\text{A16})$$

We get

$$\frac{1}{K_c(T)} \frac{\partial K_c(T)}{\partial x} = \phi_2 \frac{\partial T}{\partial x}, \quad (\text{A17})$$

where

$$\phi_2 = \left(\frac{A_1}{B} - \frac{A_3}{T} - \frac{A_4 B}{T^2} - \frac{2A_5 B^2}{T^3} \right). \quad (\text{A18})$$

$(\partial Y_O/\partial x)$ obtained in Eq. (A16) is substitute in Eq. (A13), and one obtains,

$$\frac{(\partial T/\partial x)}{(\partial \rho/\partial x)} = \frac{1}{\rho} \left[\frac{-Y_O(1-Y_O)(\bar{E}_{vib}^{eq} - RT/2 - h^0) + RT(1+Y_O)(2-Y_O)}{R/2(5+Y_O)(2-Y_O) + (1-Y_O)C_{vib}(T)(2-Y_O) - (\bar{E}_{vib}^{eq} - RT/2 - h^0)Y_O(1-Y_O)\phi_2} \right], \quad (\text{A19})$$

and $(\partial Y_O/\partial x)/(\partial \rho/\partial x)$ is calculated by substituting Eq. (A19) into Eq. (A16),

$$\frac{(\partial Y_O/\partial x)}{(\partial \rho/\partial x)} = \left[\frac{\phi_2[-Y_O(1-Y_O)(\bar{E}_{vib}^{eq} - RT/2 - h^0) + RT(1+Y_O)(2-Y_O)]}{R/2(5+Y_O)(2-Y_O) + (1-Y_O)C_{vib}(T)(2-Y_O) - (\bar{E}_{vib}^{eq} - RT/2 - h^0)Y_O(1-Y_O)\phi_2} - 1 \right] \frac{Y_O(1-Y_O)}{\rho(2-Y_O)}. \quad (\text{A20})$$

With the substitution of Eq. (A19) and (A20) into Eq. (A11), we have the final desired result,

$$\begin{aligned} \left(\frac{\partial P}{\partial \rho} \right)_s &= \left[\frac{R(1+Y_O)[-Y_O(1-Y_O)(\bar{E}_{vib}^{eq} - RT/2 - h^0) + RT(1+Y_O)(2-Y_O)]}{R/2(5+Y_O)(2-Y_O) + (1-Y_O)C_{vib}(T)(2-Y_O) - (\bar{E}_{vib}^{eq} - RT/2 - h^0)Y_O(1-Y_O)\phi_2} \right] \\ &+ \left[\frac{RT\phi_2[-Y_O(1-Y_O)(\bar{E}_{vib}^{eq} - RT/2 - h^0) + RT(1+Y_O)(2-Y_O)]}{R/2(5+Y_O)(2-Y_O) + (1-Y_O)C_{vib}(T)(2-Y_O) - (\bar{E}_{vib}^{eq} - RT/2 - h^0)Y_O(1-Y_O)\phi_2} - RT \right] \frac{Y_O(1-Y_O)}{(2-Y_O)} \\ &+ RT(1+Y_O). \end{aligned} \quad (\text{A21})$$

At the throat, $(dA/dx)=0$, and from Eq. (A3), $u_t^2 = (\partial P/\partial \rho)_s$, which is a function of T, Y_O . Consequently, the enthalpy given by Eq. (3) may also be written as a function of T, Y_O . In order to determine the couple $T_t, Y_{O,t}$ which verify the conservation of enthalpy, we integrate numerically with the Runge-Kutta method the ratio, $(\partial Y_O/\partial x)/(\partial T/\partial x) = f(T, Y_O)$ given by Eqs. (A19) and (A20). The initial conditions for the numerical integration are T_r and $Y_{O,r}$. We choose an arbitrary value of T and calculate the corresponding value of Y_O until the conservation of enthalpy is verified,

$$\begin{aligned} h_r &= (1-Y_{O,t})\bar{E}_{vib}^{eq}(T_t) + Y_{O,t}h^0 \\ &+ \frac{(7+3Y_{O,t})}{2} RT_t + \frac{u_t^2(T_t)}{2}. \end{aligned} \quad (\text{A22})$$

From the law of mass action, the mass density can be calculated, and the equilibrium mass flow is determined.

The singularity in Eq. (60) is removed, assuming that the flow is in equilibrium until the cross section corresponding to a frozen Mach number is slightly bigger than unity. For $M_i = (1+\epsilon)$, the velocity is $u_i^2 = [RT_i(1+Y_{O,i})(7+3Y_{O,i})/$

$(5+Y_{O,i})](1+\epsilon)^2$. The temperature T_i is calculated by integrating $(\partial Y_O/\partial x)/(\partial T/\partial x)$ until the couple T_i and $Y_{O,i}$ verify the conservation of enthalpy. The mass density ρ_i is calculated from the law of mass action, and the position x_i from the mass conservation.

¹R. J. Rubin and K. E. Shuler, *J. Chem. Phys.* **25**, 59, 68 (1956); R. Herman and K. E. Shuler, *ibid.* **29**, 366 (1958); K. E. Shuler, *Phys. Fluids* **2**, 442 (1959); K. E. Shuler, *J. Chem. Phys.* **32**, 1692 (1960); K. E. Shuler and G. H. Weiss, *ibid.* **45**, 1105, 1110 (1966).

²H. J. Kolker, *J. Chem. Phys.* **44**, 582 (1966); C. C. Rankin and J. C. Light, *ibid.* **46**, 1305 (1967); N. S. Snider, *ibid.* **45**, 3299 (1966); R. E. Center and G. E. Caledonia, *ibid.* **57**, 3763 (1972); M. Tabor, R. D. Levine, A. Ben-Shaul, and J. I. Steinfeld, *Mol. Phys.* **37**, 141 (1979).

³E. Montroll and K. E. Shuler, *Adv. Chem. Phys.* **1**, 369 (1958); S. H. Lin, *J. Chem. Phys.* **61**, 3810 (1974); V. M. Kenre, *Phys. Rev. A* **16**, 766 (1977); M. Tabor, R. D. Levine, A. Ben-Shaul, and J. I. Steinfeld, *Mol. Phys.* **37**, 141 (1979); J. Troe, *J. Chem. Phys.* **73**, 3205 (1980).

⁴K. E. Shuler and R. Zwanzig, *J. Chem. Phys.* **33**, 1778 (1960); F. H. Mies, *ibid.* **40**, 523 (1964); K. Takayanagi, *Adv. At. Mol. Phys.* **1**, 149 (1965); D. Secret and B. R. Johnson, *J. Chem. Phys.* **45**, 4556 (1966); H. K. Shin, *ibid.* **49**, 3964 (1968); D. Rapp and T. Kassal, *Chem. Rev.* **69**, 61 (1969); D. J. Kouri and C. A. Wells, *J. Chem. Phys.* **60**, 2296 (1974); G. D. Billing, *ibid.* **84**, 2593 (1986); T. Ree and H. K. Shin, *ibid.* **84**, 5545 (1986).

⁵A. J. Banks, D. C. Clary, and H. J. Werner, *J. Chem. Phys.* **84**, 3788

- (1986); D. W. Schwenke and D. G. Truhlar, *ibid.* **88**, 4800, (1988); M. H. Alexander, *ibid.* **99**, 7725 (1993); F. A. Gianturco and A. Storozhev, *ibid.* **101**, 9624 (1994); F. M. Tao, S. Drucker, R. C. Cohen, and W. Klemperer, *ibid.* **101**, 8680 (1994).
- ⁶J. M. Robinson, D. J. Pearson, R. A. Copeland, and F. F. Crim, *J. Chem. Phys.* **83**, 4516 (1985); J. M. Robinson, K. J. Rensberger, and F. F. Crim, *ibid.* **84**, 220 (1986); K. J. Rensberger, J. M. Robinson, and F. F. Crim, *ibid.* **86**, 1340 (1987); K. M. Beck and R. J. Gordon, *ibid.* **87**, 5681 (1987); K. J. Rensberger, J. T. Blair, F. Weinhold, and F. F. Crim, *ibid.* **91**, 1688 (1989); P. D. Magil, T. P. Scott, N. Smith, and D. E. Pritchard, *ibid.* **90**, 7195 (1989); J. M. Price, J. A. Mack, C. A. Rogaski, and A. M. Wodtke, *Chem. Phys.* **175**, 83 (1993); I. J. Wysong, *J. Chem. Phys.* **101**, 2800 (1994).
- ⁷K. E. Shuler and L. Goldstein, *J. Chem. Phys.* **28**, 700 (1958); E. W. Montroll and K. E. Shuler, *ibid.* **26**, 454 (1957); J. Ross and P. Mazur, *ibid.* **35**, 19 (1961); S. P. Heims, *ibid.* **38**, 603 (1963); J. Keck and C. Carrier, *ibid.* **43**, 2284 (1965); B. Widom, *Science* **148**, 1555 (1965); B. Shizgal, *J. Chem. Phys.* **7**, 3915 (1972); J. E. Dove and D. G. Jones, *ibid.* **55**, 1531 (1971); J. Keizer, *ibid.* **61**, 361 (1974); R. K. Boyd, *Chem. Rev.* **77**, 93 (1977); J. E. Dove and S. Raynor, *J. Phys. Chem.* **83**, 127 (1979); C. Lim and D. G. Truhlar, *J. Chem. Phys.* **87**, 2683 (1983); H. Teitelbaum, *Chem. Phys.* **124**, 55 (1988); B. D. Landrum and G. V. Candler, *J. Thermophys. Heat Trans.* **6**, 643 (1992).
- ⁸J. T. Yardley, *Introduction to Molecular Energy Transfer* (Academic, New York, 1980); J. F. Clarke and McChesney, *Dynamics of Relaxing Gases* (Butterworths, London, 1976); J. D. Lambert, *Vibrational and Rotational Relaxation in Gases* (Clarendon, Oxford, 1977); C. Park, *Nonequilibrium Hypersonic Aerothermodynamics* (Wiley, New York, 1990).
- ⁹K. Huang, D. G. Truhlar, and N. C. Blais, *J. Chem. Phys.* **86**, 2697 (1987).
- ¹⁰H. Itoh, M. Koshi, T. Asaba, and H. Matsui, *J. Chem. Phys.* **82**, 4911 (1985).
- ¹¹D. A. Gonzales and P. L. Varghese, *J. Thermophys. Heat Trans.* **8**, 236 (1994); *J. Phys. Chem.* **97**, 7612 (1993).
- ¹²M. Heymann, H. Hippler, H. J. Plach, and J. Troe, *J. Chem. Phys.* **87**, 3867 (1987); P. H. Paul, J. L. Durant, J. A. Gray, and M. R. Furlanetti, *ibid.* **102**, 8378 (1995); K. Koura, *ibid.* **77**, 5141 (1982); T. L. Mazely and M. A. Smith, *ibid.* **89**, 2048 (1988); J. V. Michael and K. P. Lim, *ibid.* **97**, 3228 (1992); R. Paul, *J. Phys. Chem.* **99**, 8472 (1995).
- ¹³R. Brun, *Transport dans les Ecoulements Gazeux* (Masson, Paris, 1986); J. A. Owczarek, *Fundamentals of Gas Dynamics* (International Textbook, Scranton, 1964); J. D. Anderson, *Modern Compressible Flow* (McGraw-Hill, New York, 1982); Y. V. Stupochenko, S. A. Losev, and A. I. Ospov, *Relaxation in Shock Waves* (Springer, New York 1967); W. G. Vincenti and C. H. Kruger, *Introduction to Physical Gas Dynamics* (Wiley, New York, 1965).
- ¹⁴S. Sazhin, P. Wild, C. Leys, D. Toebaert, and E. Sazhina, *J. Phys. D: Appl. Phys.* **26**, 1872 (1993); S. Sazhin, P. Wild, E. Sazhina, M. Makhlof, C. Leys, and D. Toebaert, *Opt. Las. Tech.* **26**, 191 (1994).
- ¹⁵L. Mirabo, Y. P. Raizer, and S. T. Surzhikov, *High Temperature* **33**, 11 (1995); E. S. Oran, T. R. Young, J. P. Boris, and A. Cohen, *Combust. Flame* **40**, 135 (1982).
- ¹⁶M. Capitelli, *Nonequilibrium Vibrational Kinetics* (Springer, Berlin, 1986); S. Longo, G. Comunale, C. Gorse, and M. Capitelli, *Plasma Chem. Plasma Proc.* **13**, 685 (1993); E. E. Nikitin, A. I. Osipov, and S. Y. Uman-skii, *Revs. Plasma Chem.* **2**, 1 (1994); A. Garscadden and R. Nagpal, *Plasma Source Sci. Tech.* **4**, 268 (1995).
- ¹⁷S. M. Ruffin and C. Park, *J. Space Rockets* **30**, 59 (1993); S. P. Sharma, S. M. Ruffin, W. D. Gillespie, S. A. Meyer, and L. W. Yates, *J. Thermophys. Heat Transfer* **7**, 261 (1993).
- ¹⁸F. Lordet, J. G. Méolans, A. Chauvin, and R. Brun, *Shock Waves* **4**, 299 (1995).
- ¹⁹S. Kato, *J. Chem. Phys.* **83**, 1085 (1985); R. Schinke and G. H. F. Diercksen, *ibid.* **83**, 4516 (1985); G. D. Billing and M. Cacciatore, *Chem. Phys. Lett.* **86**, 20 (1982); G. D. Billing, *J. Chem. Phys.* **84**, 2593 (1986); A. J. Banks and D. C. Clary, *ibid.* **86**, 802 (1987); A. J. Banks, D. C. Clary, and H. J. Werner, *ibid.* **84**, 3788 (1986); T. Ree and H. K. Shin, *ibid.* **84**, 5545 (1986); R. Steckler, D. G. Truhlar, and B. C. Garrett, *ibid.* **84**, 6712 (1986); A. J. Banks and D. C. Clary, *ibid.* **86**, 802 (1987); G. D. Billing and R. E. Kolesnick, *Chem. Phys.* **200**, 382 (1992).
- ²⁰J. M. Jackson and N. F. Mott, *Proc. R. Soc. London Ser. A* **137**, 703 (1932).
- ²¹E. W. Montroll and K. E. Shuler, *J. Chem. Phys.* **26**, 454 (1957); H. C. Anderson, I. Oppenheim, K. E. Shuler, and G. H. Weiss, *ibid.* **81**, 3012 (1964).
- ²²L. Landau and E. Teller, *Phys. Z. Sowjetunion* **10**, 34 (1936).
- ²³R. N. Schwartz, Z. Slawsky, and K. F. Herzfeld, *J. Chem. Phys.* **20**, 1591 (1952).
- ²⁴R. N. Schwartz and K. F. Herzfeld, *J. Chem. Phys.* **22**, 767 (1954); D. B. Sorensen, *ibid.* **57**, 5241 (1972); M. H. Alexander, *ibid.* **59**, 6254 (1979).
- ²⁵C. E. Treanor, R. G. Rich, and R. G. Rehm, *J. Chem. Phys.* **4**, 1798 (1968).
- ²⁶J. G. Méolans, and A. H. Chauvin, AIAA Paper 91-1340 1991; *Physica* **84C**, 432 (1976).
- ²⁷P. Hammerling, J. D. Teare, and B. Kivel, *Phys. Fluids* **2**, 422 (1959).
- ²⁸C. E. Treanor and P. V. Marrone, *Phys. Fluids* **5**, 1022 (1962).
- ²⁹P. V. Marrone and C. E. Treanor, *Phys. Fluids* **6**, 1215 (1963).
- ³⁰J. H. Kiefer and J. C. Hajduk, *Chem. Phys.* **38**, 329 (1979).
- ³¹A. Kafri and R. D. Levine, *J. Chem. Phys.* **86**, 2697 (1987).
- ³²C. Rebick and R. D. Levine, *J. Chem. Phys.* **58**, 3942 (1973).
- ³³J. H. Kiefer, H. P. Joosten, and P. G. Breshears, *Chem. Phys. Lett.* **30**, 424 (1975).
- ³⁴M. Ramakrishna and S. V. Babu, *Chem. Phys.* **35**, 259 (1979).
- ³⁵M. Ramakrishna and S. V. Babu, *J. Chem. Phys.* **68**, 163 (1978).
- ³⁶K. Koura, *Phys. Fluids* **6**, 3485 (1994); B. L. Haas and I. D. Boyd, *Phys. Fluids A* **5**, 478 (1992).
- ³⁷C. Park, *J. Thermophys. Heat Transfer* **2**, 8; **3**, 233 (1988).
- ³⁸K. Nanbu, *J. Phys. Soc. Jpn.* **40**, 1391 (1976); R. E. Center and G. E. Caledonia, *J. Chem. Phys.* **57**, 3763 (1972); A. Chiroux de Gavelle de Roany, C. Flament, J. W. Rich, V. V. Subramaniam, and R. Warren, AIAA *J.* **31**, 119 (1992).
- ³⁹D. Zeitoun, E. Boccaccio, M. Druget, and M. Imbert, AIAA *J.* **132**, 333 (1994); D. Tirumalesa, AIAA *J.* **5**, 254 (1966).
- ⁴⁰J. C. Light, J. Ross, and K. E. Shuler, in *Kinetic Processes in Gases and Plasma*, edited by A. R. Hochstim (Academic, New York, 1969).
- ⁴¹G. Herzberg, *Spectra of Diatomic Molecules* (Van Nostrand, New York, 1950).
- ⁴²C. Park, *J. Thermophys. Heat Transf.* **3**, 385 (1993).
- ⁴³R. S. Brokaw, *Proceedings of the Conference on Physical Chemistry in Aerodynamics and Space Flight, 1961* (unpublished), Vol. 3, p. 238.
- ⁴⁴A. A. Radzig and B. M. Smirnov, *Springer Series in Chemical Physics* (Springer-Berlin, 1985), Vol. 31.
- ⁴⁵S. J. Cubley and Mason, *Phys. Fluids* **18**, 1109 (1975).
- ⁴⁶M. Camac, *J. Chem. Phys.* **34**, 448 (1961).
- ⁴⁷R. C. Millikan and D. R. White, *J. Chem. Phys.* **39**, 3209 (1963).
- ⁴⁸J. Kunc, *J. Phys. B. Mol. Opt. Phys.* **24**, 3741 (1991).
- ⁴⁹G. Bader and P. Deuflhard, *Numer. Math.* **41**, 373 (1983).
- ⁵⁰W. H. Press, S. A. Teukolsky, W. T. Vetterling, and B. P. Flannery, *Numerical Recipes in Fortran*, 2nd ed. (Cambridge University, Cambridge, 1992).
- ⁵¹C. J. F. Ridders, *Adv. Eng. Software* **4**, 75 (1982).